

Dynamics of detonations with a constant mean flow divergence

Bijan Borzou and Matei I. Radulescu[†]

Department of Mechanical Engineering, University of Ottawa, ON K1N 6N5, Canada

(Received xx; revised xx; accepted xx)

The present work addresses the question of whether mean field macroscopic models are suitable to describe the dynamics of real cellular detonations. This question is posed in the framework of detonations with stream-tube area divergence that is kept constant, as to generate attenuated detonations in quasi-steady state. An exponential horn geometry is used, in order to keep the source term due to geometrical divergence constant in the governing equations of mean flow, and hence permit to establish steady travelling waves with constant losses. The experiments were conducted in two mixtures $2\text{C}_2\text{H}_2+5\text{O}_2+21\text{Ar}$, characterized by a relatively weak instability, and $\text{C}_3\text{H}_8+5\text{O}_2$, characterized by a much more unstable cellular structure. The experiments demonstrated that such quasi-steady state detonations can be realized. The experiments permitted a unique detonation speed - divergence scaling laws to be developed. Three types of models were tested: empirical models tuned to the experiments, steady wave predictions based on the underlying chemistry and inviscid non-steady multi-dimensional simulations. First, it was shown that effective reaction models can be tuned against such experiments. This shows that a mean field description can be used to capture the dynamics of detonations with a global divergence in the reaction zone. Secondly, unsteady cellular simulations of the inviscid reactive gasdynamic equations were performed for the $2\text{C}_2\text{H}_2+5\text{O}_2+21\text{Ar}$ system with a chemical kinetic model derived from the underlying multi-step chemical decomposition of this fuel. It was shown that the simulations were in excellent agreement with experiment for moderate divergence rates, but some discrepancies were observed at near limit conditions. Overall, it can be concluded that inviscid type calculations can reproduce the experimental results correctly in this type of mixtures. The unsteady simulations also served to comment on the relevancy of the steady state models to capture inviscid cellular detonation dynamics. It was found that the cellular simulations of inviscid detonations lead to departures from the steady wave prediction. The unstable cellular simulations gave rise to larger velocity deficits at a given global divergence rate, as well as to a smaller maximum divergence rate. This unambiguous comparison highlighted that inviscid cellular detonations have narrower limits than predicted by steady models. Finally, the experiments obtained in the much more unstable mixture $\text{C}_3\text{H}_8+5\text{O}_2$ showed that there were very large departures between the experimentally derived $D - K$ curve and the prediction of steady wave propagation based on the underlying chemistry. The reason for this discrepancy is likely to be due to the importance of diffusive processes in the burn-out of the the non-reacted pockets during the propagation, as observed from the reaction zone visualization. Furthermore, the empirical tuning of a global induction-reaction model to describe the experimental trends revealed that the effective activation energy was lower by 70%. This confirms previous observations that diffusive processes in highly unstable detonations are responsible for reducing the thermal ignition character of the gases processed by the detonation front (Radulescu *et al.* 2007b).

[†] Email address for correspondence: matei@uottawa.ca

Key words: Compressible Flows-Detonation waves; Reacting Flows-Detonations

1. Detonations with lateral flow divergence

The rate of propagation of one-dimensional detonation waves in the presence of non-ideal effects (mass divergence, unsteadiness, diffusive transfer of mass, momentum and energy) is generally a consequence of a balance between the rate of exothermity in the reaction zone, which dictates how fast pressure waves are amplified within the reaction zone in order to sustain the lead shock, and the losses, which have the opposite effect (Fickett & Davis 1979; Bdzil & Stewart 2007). Such models are extensions of the classical one-dimensional Zeldovich-Von-Neumann-Doering (ZND) and rely on the generalized Chapman-Jouguet theory (Fickett & Davis 1979; Bdzil & Stewart 2007). The framework of these theoretical models is mainly one-dimensional. In gases, real detonations are multi-dimensional and take on a complex cellular structure (Lee 2008; Shepherd 2009). The question that arises is whether current models based on extensions of the ZND formulation are relevant to real detonations at the macro-scale description, even in an approximate way. This is the question we wish to answer in the present paper.

Analysis of complex detonation structures in gases revealed that although the front is highly unstable, it recovers qualitatively a quasi-one-dimensional average structure analogous to the ZND structure, with an embedded sonic surface (Radulescu *et al.* 2007*b*). It thus appears that, with the appropriate kinetic description for the average reaction zone structure dictated by an effective rate of energy release, the ZND model with its extensions may be an appropriate framework to model detonations (Radulescu *et al.* 2007*b*).

The present study focuses on the dynamics of detonations with mass divergence at the macro-scale. We wish to determine if steady models based on the ZND structure with mass divergence can be used to provide models for such detonations.

Mass divergence in the reaction zone of detonations has been proposed to be one of the main mechanisms of detonation attenuation and possible extinction in various geometries (Klein *et al.* 1995). The best example is for cylindrical and spherical detonations. Although these are never steady, as the rate of divergence decays with distance from the center of symmetry, quasi-steady first-principles models based on extensions of the ZND model using the generalized Chapman-Jouguet theory have been formulated and compared to experiments of detonation initiation (He & Clavin 1994; Kasimov & Stewart 2005). Although order of magnitude agreement was obtained for the critical initiation energies, it was also argued that the comparison is difficult in view of important unsteady effects neglected in the models (Eckett *et al.* 2000). Eckett *et al.* (2000) proposed that critical ignition can be predicted by consideration of the critical expansion rate of the gases undergoing ignition. Calculations based on extensions of the ZND theory to account for the total mass divergence were found to rationalize some experimental trends, but still required some empirical coefficients to match the model to the blast wave solution in the close field. The question of whether the ZND model and its extensions can capture real detonation dynamics remains an open one for these problems.

Mass divergence in the reaction zone of detonations is also believed to control the problem of detonation diffraction at an abrupt area change (Lee 1984; Edwards *et al.* 1979; Arienti & Shepherd 2005; Mitrofanov & Soloukhin 1965; Vasil'ev 1994). Models based on extensions of the ZND model to account for a critical expansion of the flow

undergoing ignition have also been attempted by Shepherd and his collaborators (Arienti & Shepherd 2005; Klein *et al.* 1995; Schultz 2000). Nevertheless, a first principle predictive capability was not possible, since the closure required again empirical coefficients for matching.

Mass divergence in the reaction zone of detonations is also believed to control the detonation dynamics in narrow tubes, where the viscous boundary layers developing on the tube walls act as a mass sink to the core flow. The divergence of the streamlines in the reaction zone results in a curved detonation front experiencing a velocity deficit (Dupre *et al.* 1991; Chinnayya *et al.* 2013; Moen *et al.* 1981). Chao *et al.* (2009), Camargo *et al.* (2010) and Gao *et al.* (2016) attempted to compare the velocity deficits and limits observed in the experiments with predictions based on the ZND model with mass divergence. The amount of mass divergence was modelled globally using boundary layer theory using Fay's model (Fay 1959). The authors have found relatively good agreement for weakly unstable detonations, and poorer agreement for more unstable detonations. Nevertheless, there were a number of simplifying assumptions and matching constants, whose impact on the predictions have not been evaluated. Firstly, Fay's model requires as empirical input a particular length scale for evaluating the mass divergence, typically taken as the induction length or the cell length of the non-attenuated detonation. The model also assumes uniform curvature along the front, implying uniform area divergence for each stream tube in the reaction zone. A curved detonation due to wall boundary layers or permeable walls is not expected to have a unique curvature, as demonstrated by Chinnayya *et al.* (2013) numerically and theoretically by Bdzil and Stewart in the context of Detonation Shock Dynamics (DSD) (Bdzil & Stewart 2007). Further away from the axis of the channel or tube, the flow divergence departs from that along the streamline along the axis.

Mass divergence in the reaction zone of detonations can also be controlled in tubes with leaky, or porous walls. Radulescu (2003) and Radulescu & Lee (2002) have conducted an extensive experimental series in several reactive mixtures and compared their results with the predictions of the ZND model with mass divergence. In the models, the amount of mass divergence was assumed constant for all streamtubes, and evaluated from the porosity of the walls assuming choked flow. The comparison with experiment did not require further tuning parameters. Nevertheless, the assumption of constant divergence is also not realistic, as demonstrated numerically by Mazaheri *et al.* (2015) and argued above for detonations in narrow tubes and channels. These limitations diminish the value of the comparison between experiment and ZND model predictions. Nevertheless, interesting trends were observed. For weakly unstable detonations, the model predictions using the real kinetics, particularly for the critical divergence rate, were found in very good agreement with experiment. For more unstable detonations, the agreement was much poorer. The experimental detonations were found to propagate when the ZND models predicted extinction. The authors interpreted this finding as the enhancement of the burning rate in more unstable detonations by multi-dimensional effects. Later, Radulescu *et al.* (2007b) determined that the enhancement originated from the much lower effective activation energy of turbulent detonations, where turbulent mixing significantly removes much of the thermal character of ignition in the ZND model and its extensions.

Mass divergence in the reaction zone of detonations also controls the dynamics of detonations with weaker/non-reactive confinement. In condensed-phase detonations, the confiner of a finite charge always yields to the very high pressures developed in the reaction zone. Models for detonations with mass divergence have been developed for these reactive materials, see for example Fickett & Davis (1979) and Bdzil & Stewart (2007) for

a recent review. For these materials, the kinetics of the decomposition are not known from first principles. Instead, the models are calibrated from experiment. Although the models have demonstrated their extreme usefulness in describing the macro-scale structure in a bottoms-down approach, the question remains of whether models derived from first principle kinetics at small scales will continue to work at macro-scales. Although this cannot be answered for condensed phase detonations, for gases, the kinetics of gas phase reactions are relatively well known to permit such a comparison. Unfortunately, analogous experiments in the gas phase are difficult to conduct. The few experiments available have not yet been compared with first principles calculations (Dabora *et al.* 1965; Murray & Lee 1984, 1986; Vasil’ev *et al.* 1972) of the DSD type Bdzil & Stewart (2007).

The present study addresses this central problem of detonation dynamics with global mass divergence. We formulate a novel problem in which the rate of mass divergence can be kept *constant*, hence permitting steady detonations to be established. The constancy of the divergence rate is by maintaining a constant logarithmic derivative of the channel cross-sectional area with distance (see Section 2), such that the governing equations at the macro-scale quasi-1D description have a constant source term. This permits us to compare the relation between the detonation wave speed deficit and the rate of mass divergence with the prediction made by steady models, and simulations. This permits us to draw a meaningful conclusion on the adequacy of steady and unsteady multi-dimensional models on predicting the canonical problem of detonation dynamics with mass divergence.

Of particular interest is to draw this conclusion on two classes of detonations: weakly unstable and highly unstable detonations; as previous observations have revealed that the ZND model may only apply to the weakly unstable detonations (Radulescu & Lee 2002; Radulescu 2003; Chao *et al.* 2009; Camargo *et al.* 2010). Detonations labeled “Weakly unstable” in the literature are characterized by relatively weak chemical reaction rate dependence to temperature fluctuations, regular cell structures and absence of diffusive transport (Radulescu *et al.* 2007b; Sharpe 2001; Deiterding 2003; Hu *et al.* 2005). Highly unstable detonations refer to detonations with a strong sensitivity of the reaction rates to temperature, irregular detonation structures with a typical sub-structure, and reaction zones in which turbulent mixing via hydrodynamic instabilities enhance the burning rates (Radulescu *et al.* 2007b; Mazaheri *et al.* 2012). The importance of instabilities on limiting phenomena in detonations have also been quantified recently in the context of 1D detonation response to heat and frictional losses Sow *et al.* (2014). They found that the predictions made without accounting for the pulsating instabilities under-predicted the velocity deficit. The extinction limit predicted by a quasi-steady model over-predicted the amount of loss necessary for extinction. This is the opposite trend of that observed experimentally for multi-dimensional detonations as discussed above. It is presently unclear whether this result is due to the assumption of one-dimensional flow, albeit a pulsating one. These observations further suggest the role of the pulsating dynamics in controlling the limits.

To summarize, we propose a novel geometry whereby the rate of global mass divergence is stationary, which permits to establish detonations in steady state at the macro-scale. This permits an unambiguous comparison with models and numerical simulations in order to establish quantitatively whether a global quasi-1D formulation is meaningful for detonations in gases. The experiments were performed for two different mixtures characterized by weakly unstable ($2\text{C}_2\text{H}_2+5\text{O}_2+21\text{Ar}$) and highly unstable ($\text{C}_3\text{H}_8+5\text{O}_2$) cellular structures. These mixtures were among the frequent choices by the past studies looking for weakly unstable and highly unstable detonations (Shepherd 1986; Van-

dermeiren & Tiggelen 1984; Chao *et al.* 2009; Camargo *et al.* 2010; Radulescu 2003; Radulescu & Lee 2002; Strehlow & Engel 1969).

The current paper is organized as follows. Section 2 offers a brief justification of the usefulness of the *exponential horn* geometry to study quasi-steady detonations with a constant global rate of mass divergence. Section 3 provides the details of the experimental procedure and the experimental results obtained. Section 4 provides the steady travelling wave solution for a detonation with constant mass divergence for the two mixtures. Section 5 presents the numerical simulation results of the cellular detonation dynamics in diverging channels for the weakly unstable detonation. Comparison of the different models with experiment is reported in Section 6 along with further discussion on the implication of the results.

2. Quasi-1D flow with lateral mass-divergence

The exact equations of gasdynamics in multiple dimensions for a N -component system, which neglect transport terms, are the so-called reactive Euler equations. The usual continuity, momentum conservation and energy conservation following a fluid particle are:

$$-\frac{1}{\rho} \frac{D\rho}{Dt} = \nabla \cdot \mathbf{u} \quad (2.1)$$

$$\rho \frac{D\mathbf{u}}{Dt} = -\nabla p \quad (2.2)$$

$$\frac{De}{Dt} = -\frac{p}{\rho^2} \frac{D\rho}{Dt} \quad (2.3)$$

where $D/Dt = \partial/\partial t + \mathbf{u} \cdot \nabla$ is the material derivative and the symbols have their usual meaning (Williams 1985). These need to be complemented by an appropriate equation of state for the internal energy e of the form:

$$e = e(p, \rho, Y_1, Y_2, \dots, Y_i, \dots, Y_N) \quad (2.4)$$

and the appropriate kinetics for the evolution of the mass fractions Y_i 's of each of the system's N components:

$$\frac{DY_i}{Dt} = \frac{\omega_i}{\rho} \quad (2.5)$$

When a quasi-1D formulation is sought in a duct (or streamtube) of cross-section $A(x)$, the variables take the meaning of transverse averages (or streamtube variables) and the equations remain unchanged, with $D/Dt = \partial/\partial t + u\partial/\partial x$. The divergence of the velocity field in the continuity equation (2.1), which describes the rate of volume change of a fluid element per unit volume, can be expressed as two contributions.

$$\nabla \cdot \mathbf{u} = \frac{\partial u}{\partial x} + \dot{\sigma}_A \quad (2.6)$$

The first is the usual rate of strain of a fluid element in the flow direction x , and the second, $\dot{\sigma}_A$, is the rate of strain in the transverse direction (Whitham 1974; Williams 1985):

$$\dot{\sigma}_A \equiv u \frac{d(\ln A)}{dx} \quad (2.7)$$

This term plays a fundamental role in both inert (Whitham 1974) and reactive gasdynamics (Fickett & Davis 1979), as it provides the rate of expansion or compression

of a fluid element due to geometrical effects. For such quasi-one-dimensional flows, the conservation laws are best cast in characteristic form, which, after some manipulation and basic thermodynamic identities (Williams 1985; Kao 2008; Wood & Kirkwood 1957), yield:

$$\frac{1}{\rho c^2} \frac{D_{\pm} p}{Dt} \pm \frac{1}{c} \frac{D_{\pm} u}{Dt} = \dot{\sigma} - \dot{\sigma}_A \quad (2.8)$$

where the derivatives

$$\frac{D_{\pm}}{Dt} = \frac{\partial}{\partial t} + (u \pm c) \frac{\partial}{\partial x} \quad (2.9)$$

are taken along the path of forward facing C_+ and rear facing C_- characteristics, given respectively by $dx/dt = u \pm c$. The thermicity $\dot{\sigma}$ denotes the gasdynamic effect of chemical reactions or other relaxation phenomena on the rate of pressure and speed changes along the family of characteristics. We immediately remark that the effect of transverse flow divergence $\dot{\sigma}_A$ has precisely the opposite effect to the thermicity $\dot{\sigma}$ on modulating the strength of acoustic waves along the characteristic paths.

The thermicity in its most general form is given by:

$$\dot{\sigma} = -\frac{\rho}{C_p} \left(\frac{\partial v}{\partial T} \right)_{p, Y_i} \sum_{i=1}^N \left(\frac{\partial h}{\partial Y_i} \right)_{p, \rho, Y_j, j \neq i} \frac{DY_i}{Dt} \quad (2.10)$$

(Fickett & Davis 1979; Williams 1985; Kao 2008). This expression takes a simple and more familiar form for a reacting perfect gas with an equation of state of the form

$$p = \rho RT \quad (2.11)$$

$$e(p, \rho, Y_R, Y_P) = \frac{1}{\gamma - 1} \frac{p}{\rho} + (1 - Y_P) Q \quad (2.12)$$

where Y_R and Y_P are the mass fractions of the reactants and products, respectively, γ is the isentropic exponent and Q is the chemical energy released during the reaction (Fickett & Davis 1979):

$$\dot{\sigma} = \frac{(\gamma - 1)\rho Q}{\gamma p} \frac{DY_P}{Dt} \quad (2.13)$$

In the present paper, we will deal with flows for which the source term appearing in the quasi-one-dimensional formulation for a streamtube or in a tube of cross-sectional area $A(x)$, namely:

$$K \equiv \frac{d(\ln A)}{dx} \quad (2.14)$$

is a *constant*. The source term being a constant permits us to establish a steady (on average) detonation structure, as can be anticipated since the source is neither a function of space nor time. In the current work, we study the dynamics of detonations in a channel with a constant logarithmic derivative K , i.e., a channel with a cross-section varying exponentially with distance. This is known as an *exponential horn* in acoustics, since, in the absence of chemical reactions, acoustic waves will have constant amplification factors by virtue of (2.8).

3. Experiments

3.1. Experimental setup

Figure 1 shows the schematic of the 3.4-m-long rectangular channel used for the experiments in this paper (Maley 2015). The channel is made of aluminium. The internal

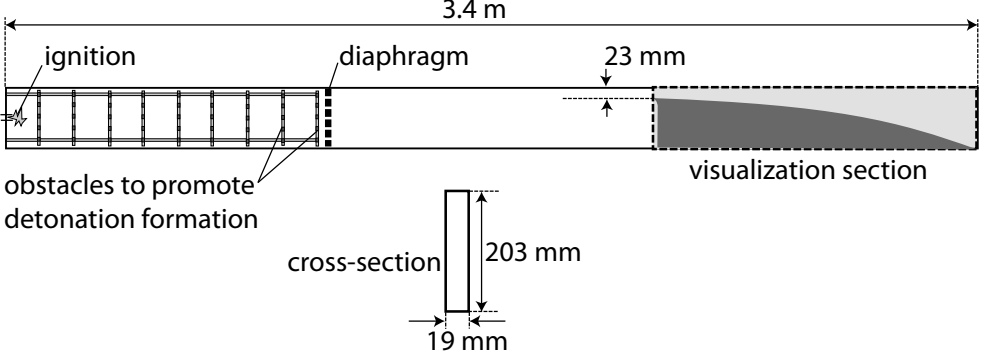


FIGURE 1. A schematic of the experimental apparatus to study diverging detonations.

height and width of the channel are 203 mm and 19 mm respectively. This internal width was found to be the optimum value to suppress the transverse perturbations and thus approximate the detonation cellular dynamics as two-dimensional (Bhattacharjee 2013).

The channel had three identical sections (Fig. 1). The diverging ramp was placed in the third section, which was equipped with glass panels allowing to visualize the detonation front evolution. Two exponentially diverging ramps were used for the tests, which permitted to correct for boundary layer losses in a thin channel geometry, as described later. A long ramp (with 1-m-length and $K = \frac{1}{A} \frac{dA}{dx} = 2.302 \text{ m}^{-1}$) and a short ramp (with 0.5-m-length and $K = \frac{1}{A} \frac{dA}{dx} = 4.605 \text{ m}^{-1}$) were used. At the entrance of the diverging section, the initial opening was 23 mm in height. A "cookie-cutter" entrance was used in order to isolate the detonation front entering the diverging section. The diverging ramp was machined from a sheet of polyvinyl-chloride (PVC).

The detonation was initiated by two different methods in the first section of the channel. In the first method, a powerful spark from capacitor discharge was used. Its discharge characteristics are described in detail by Bhattacharjee (2013). The capacitor bank stored approximately 1000 J at a charging voltage of approximately $V_0 = 32 \text{ kV}$ and its discharge characteristic time was less than $2 \mu\text{s}$. The ensuing strong blast wave generated by the hot plasma generated a high-speed deflagration wave. A wire-mesh grid was installed in the first section of the tube in order to ensure the rapid transition of the deflagration wave to a detonation. This method, however, was not successful in the experiments conducted with the acetylene mixture at initial pressures below 8 kPa. For these conditions, a more sensitive reactive driver was used in the first section of the channel, which was separated from the test mixture by a thin Mylar diaphragm (see Fig. 1). The driver gas used was $\text{C}_2\text{H}_4 + 3\text{O}_2$. The driver gas was ignited using the same capacitor discharge as described above, in which a detonation was established. This incident detonation wave was found to transmit successfully into the test mixture.

The mixtures tested were $2\text{C}_2\text{H}_2 + 5\text{O}_2 + 21\text{Ar}$ and $\text{C}_3\text{H}_8 + 5\text{O}_2$. The mixtures were prepared by the method of partial pressures in a separate mixing tank. The mixtures were typically left to mix over a period of at least 24 hours prior to an experiment. Before an experiment, the channel was first evacuated to a pressure below 100 Pa prior to the injection of the test mixture. The experiments were performed at ambient room temperature of $20 \pm 2^\circ\text{C}$. The sensitivity of the test mixtures was controlled by varying the initial pressure of the gases.

The visualization of the detonation wave front evolution in the diverging channels was performed using a large-scale shadowgraph system described by Dennis *et al.* (2014).

A high speed Phantom V1210 camera was used for visualization. Images were recorded at resolutions of 1152 by 256 and a framing rate of approximately 42000 frames per second, yielding a time resolution of approximately 24 μ s. An exposure of 1 μ s was used. For reference, typically 20 consecutive frames were acquired to monitor the detonation passage through the test section. These frames were then post-processed in order to evaluate the speed of the lead shock between successive frames. These were recorded along the top wall only. The typical errors in evaluating these speeds, derived from the image resolution and the ability to identify the lead shock position in the photographs was approximately $\pm 2\%$ (Borzou 2016).

3.2. Results in $2C_2H_2+5O_2+21Ar$

Figure 2 shows the evolution of the detonation wave propagation for five different experiments in $2C_2H_2+5O_2+21Ar$ at different initial pressures. Each record was obtained by overlaying the shadowgraph images obtained from the high speed visualization videos of the same experiment. The detonation wave propagated from left to the right in the diverging domain. The leading shock front is identified by the thick black line, followed by a bright, corresponding to the strong chemi-luminescence of the gas at high temperatures, which is overlaid on the shadowgraph record.

At sufficiently high pressures (Fig. 2(a) and (b)), the detonation front is textured with a large number of small sized cells. Traces of the transverse waves starting from the triple points on the wave front, and extending back across the reaction zone are also observed. As the detonation progresses in the enlarging section, it acquires the expected curvature due to the geometrical divergence of the gases behind the front. With decreasing pressure, such as Fig. 2(c) and (d), the cellular structure of the front is enlarged, partly due to the lower reactivity of the gas at lower pressures (see below) and partly due to the stronger propensity for the detonation wave to be attenuated by the diverging geometry. A somewhat thicker reaction zone is also observed. The cellular structure is characterized by transverse detonations consuming the gas behind the incident shock portions of the front. This can be clearly seen in Fig. 2(d), where most of the gas accumulating as non-reacted behind the weaker portion of the shock near the bottom wall reacts very fast behind a transverse wave, which takes the form of a transverse detonation wave with fine cellular structure typical of near limit detonations reported by Gamezo *et al.* (2000). Very few non-reacted pockets are observed, with negligible volumes, as shown in Fig. 2(d). When the initial pressure was lowered below a critical value, the detonation was extinguished in the diverging channel, with a quasi-1D reaction zone decoupling from the lead shock, as shown in Fig. 2(e).

The speed of the leading front recorded along the top wall from the sequential frames is shown in Fig. 3 for the experiments shown in Fig. 2. At the higher pressures, the framing rate does not resolve the cellular structure of the front, and an essentially time-averaged speed is recorded. The experiments indicate that this speed remains constant for the entire detonation travel in the diverging channel. This confirms the concept that an exponential horn can maintain a steady travelling detonation. This shows unambiguously that a mean description is worthwhile.

At the lower pressures of 6.2 and 4.9 kPa, the large cellular structures shown in Fig. 2(c) and (d) are now better resolved. The cellular dynamics give rise to speed fluctuations of approximately 500 m/s, or 30% of the average propagation speed. In spite of these very large fluctuations typical of cellular dynamics, the average speed is approximately constant. Finally, at an initial pressure of 4.2 kPa, the lead shock is seen to continuously decay. A detonation wave can no longer remain self-sustained in the diverging section - see also Fig. 2(e) showing the absence of cellular structures.

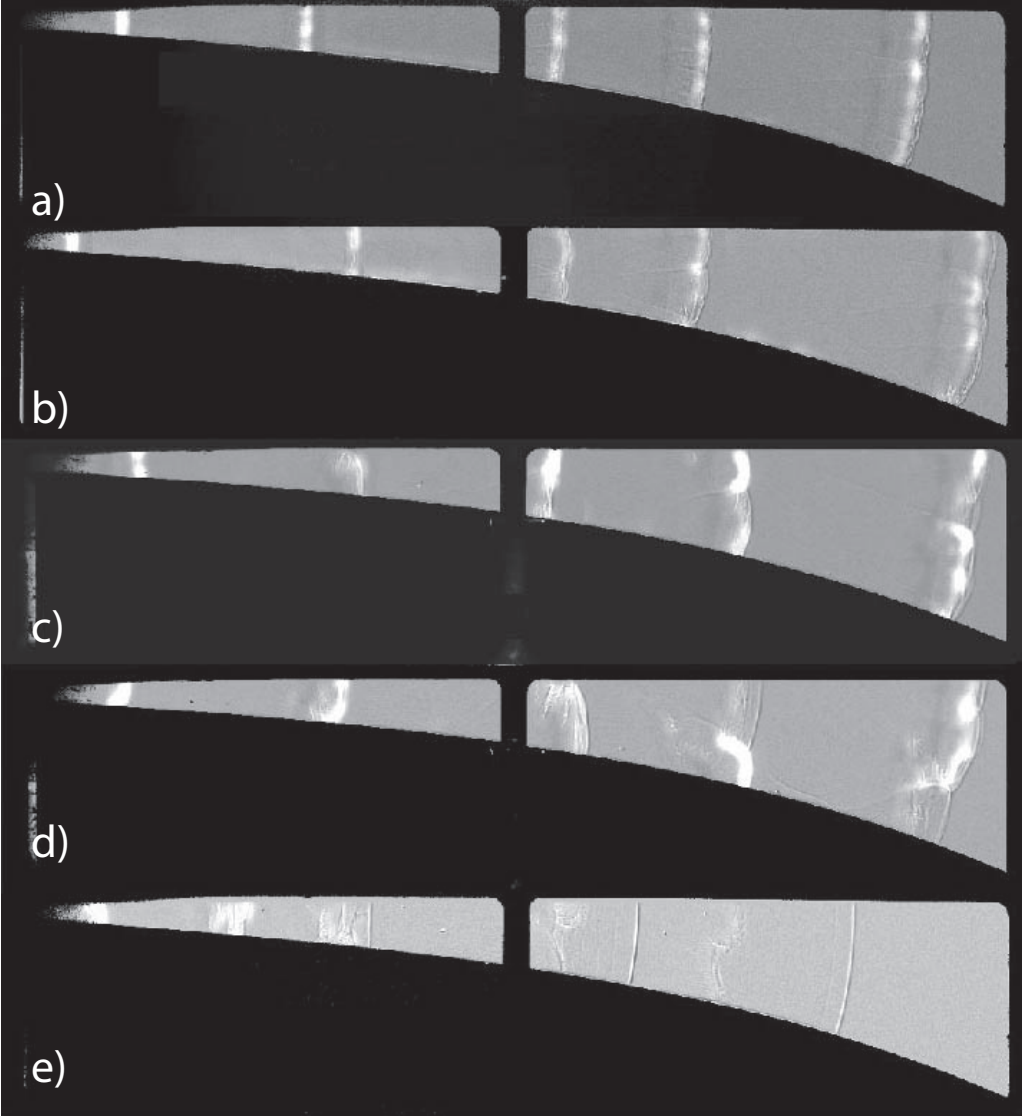


FIGURE 2. Detonation front evolution in $2\text{C}_2\text{H}_2+5\text{O}_2+21\text{Ar}$ along the long ramp at initial pressures of (a) 12.1 kPa, (b) 9 kPa, (c) 6.2 kPa, (d) 4.9 kPa and (e) 4.2 kPa.

The experiments performed with the shorter ramp with double the amount of divergence showed very similar flow fields. Fig. 4 shows the evolution of the front of the detonation, while Fig. 5 shows the recorded speeds along the top wall for four typical experiments showing the range of phenomena observed. While at the higher pressures, the detonation front has a uniform curvature and small cellular structures, the cellular structure enlarges at lower pressures. The records indicate that the cellular structure corresponds to reactive transverse waves, as documented in detail by Gamezo *et al.* (2000). The speeds record of Fig. 5 shows that for the shorter ramp, a steady detonation can also be established. Once the cellular structure can be resolved by the framing rate used (Figs. 4(c) and 5(c)), the front has variations of approximately 500 m/s, or 30% of the average propagation speed. When the pressure is sufficiently low, the detonation wave

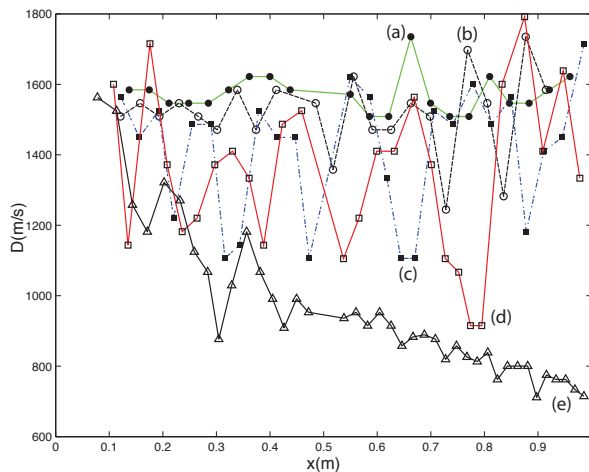


FIGURE 3. Speed of detonation front recorded along the top wall in $2\text{C}_2\text{H}_2+5\text{O}_2+21\text{Ar}$ along the long ramp at initial pressures of (a) 12.1 kPa, (b) 9 kPa, (c) 6.2 kPa, (d) 4.9 kPa and (e) 4.2 kPa, corresponding to the experiments shown in Fig. 2.

cannot propagate in the diverging section. The front consists of a decoupled shock-flame structure (Fig. 4(d)). The lead shock decays to low speeds of approximately 800 m/s by the end of the channel (Fig. 5(d)).

A summary of average speeds measured in all the experiments in $2\text{C}_2\text{H}_2+5\text{O}_2+21\text{Ar}$ on both ramps are shown in Fig. 6 as a function of the initial pressure in the mixture. The error bars represent the standard deviation of the measurements for each experiment. As expected, the error bar grows with decreasing pressure, since the cellular dynamics are better resolved. Repeat experiments are also shown. The spread between repeat experiments never exceeded 4%, which is significantly lower than the standard deviation due to the cellular dynamics fluctuations.

Also shown in the Fig. 6 is the ideal Chapman-Jouguet (CJ) detonation speed, which was obtained from chemical equilibrium calculations using the NASA CEA code (McBride & Gordon 1996). The figure shows that both the CJ speed and the experimentally determined speed drop for both large and small ramp experiments when the initial pressure is lowered. The CJ speed drops because of the enhanced dissociation in the product species at low pressures. Nevertheless, the mean shock speed recorded in the experiments also deviates from the CJ speed with a decrease in the initial pressure. This can be interpreted in terms of the gas sensitivity varying with the initial pressure. Mixtures with lower initial pressures are the ones with slower reaction rates and chemical energy release rate - see below. Therefore, the expansion cooling experienced by the shocked gas particles due to the lateral area divergence is able to decrease the shock strength and speed. Since the CJ speed represents the velocity of a steady detonation wave, the lower initial pressures result in more deviation from the CJ speed.

3.3. Results in $\text{C}_3\text{H}_8+5\text{O}_2$

The experiments performed in the $\text{C}_3\text{H}_8+5\text{O}_2$ mixture were qualitatively similar to the ones presented above for the acetylene mixture - although some fundamental differences were observed. Figs. 7 and 8 show the results for the long ramp, while Figs. 9 and 10 show the results for the short ramp. Firstly, for these mixture, a steady detonation was

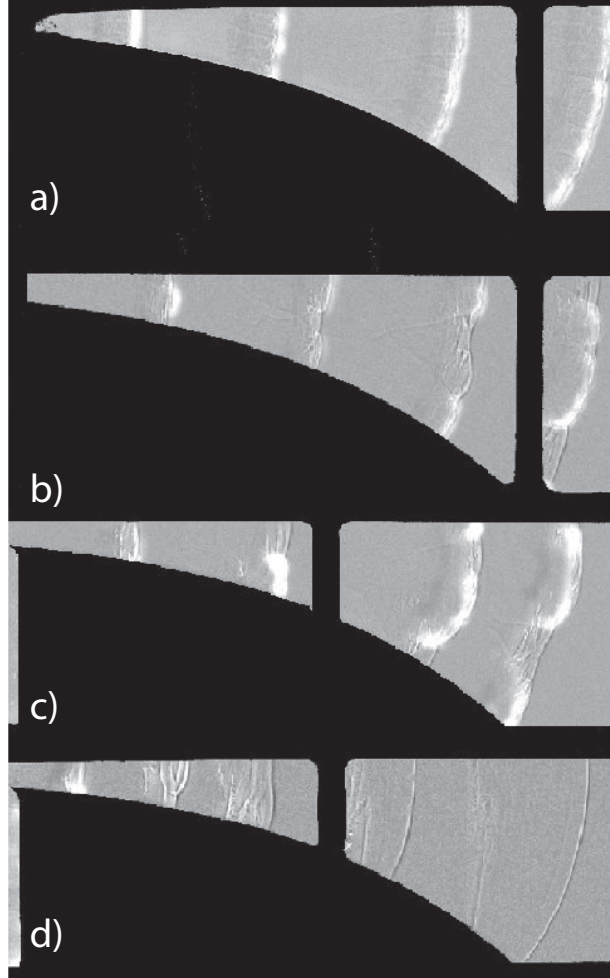


FIGURE 4. Detonation front evolution in $2\text{C}_2\text{H}_2+5\text{O}_2+21\text{Ar}$ along the short ramp at initial pressures of (a) 12.1 kPa, (b) 8.3 kPa, (c) 6.2 kPa, and (d) 4.9 kPa.

again observed in the diverging sections, confirming the appropriateness of a mean field description to model the dynamics.

The most important difference with the earlier mixture was the cellular mode of propagation, as shown in Fig. 7(d) at a sufficiently low pressure such that the cells are large enough to be well resolved. The transverse waves for this mixture appeared as non-reactive, with tongues of unreacted pockets extending downstream and sometime pinched off as pockets. This is typical of more unstable detonations (Austin 2003; Subbotin 1976; Radulescu *et al.* 2007*b*; Maxwell 2016). Nevertheless, reactive transverse waves were also sometimes observed, as shown in Fig. 9(c). These were however the exception. In order to fully address the mode of propagation of these more unstable detonations, a few Schlieren experiments were also performed for the small ramp, since the field of view of these was limited to the dimension of the mirrors (30 cm). The set-up for the Schlieren experiments is described elsewhere (Bhattacharjee 2013). Fig. 11 shows part of the front evolution for an initial pressure of 4.8 kPa. As can be clearly seen at this time and space resolution, the detonation wave takes on a characteristic cellular structure with non-reactive transverse waves (Austin 2003; Subbotin 1976; Radulescu *et al.* 2007*b*; Maxwell

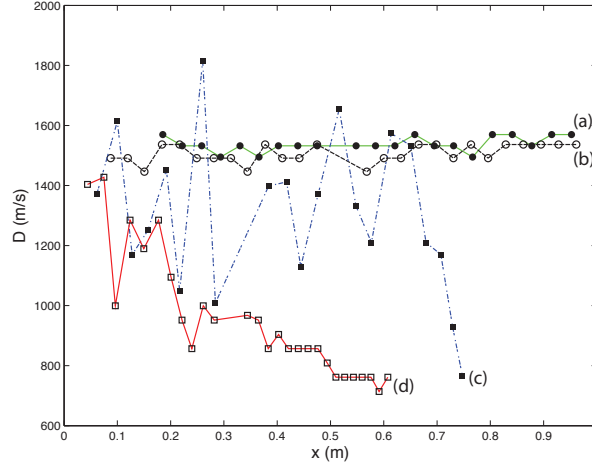


FIGURE 5. Speed of detonation front recorded along the top wall in $2C_2H_2+5O_2+21Ar$ along the short ramp at initial pressures of (a) 12.1 kPa, (b) 8.3 kPa, (c) 6.2 kPa and (d) 4.9 kPa corresponding to the experiments shown in Fig. 4.

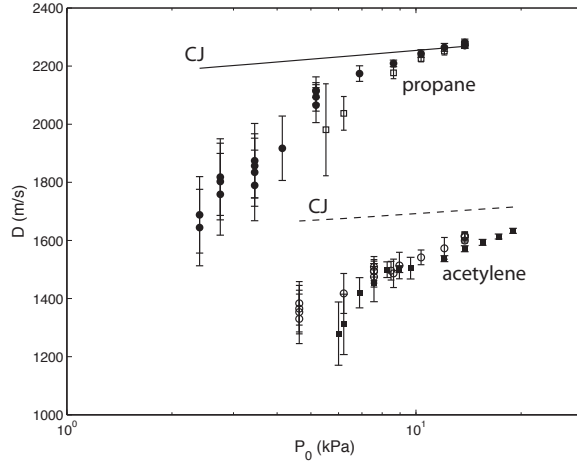


FIGURE 6. Mean detonation wave speeds along the top wall for all initial pressures permitting the sustenance of detonations experiments.

2016). Gases accumulating behind the incident shock, here the central part of the front in Fig. 11(a) accumulate as non-reacted layers of gas, which are then pinched off from transverse wave collisions (Fig. 11(c)). These pockets are then thinned out from their edges inwards through diffusive phenomena (flames).

A summary of the average speeds measured in all the experiments in $C_3H_8+5O_2$ on both ramps are shown in Fig. 6 as a function of the initial pressure in the mixture, along with the ideal Chapman-Jouguet speeds calculated with the chemical equilibrium code CEA. Similar to the acetylene experiments, the velocity deficit grows with a decreasing pressure until extinction is observed.

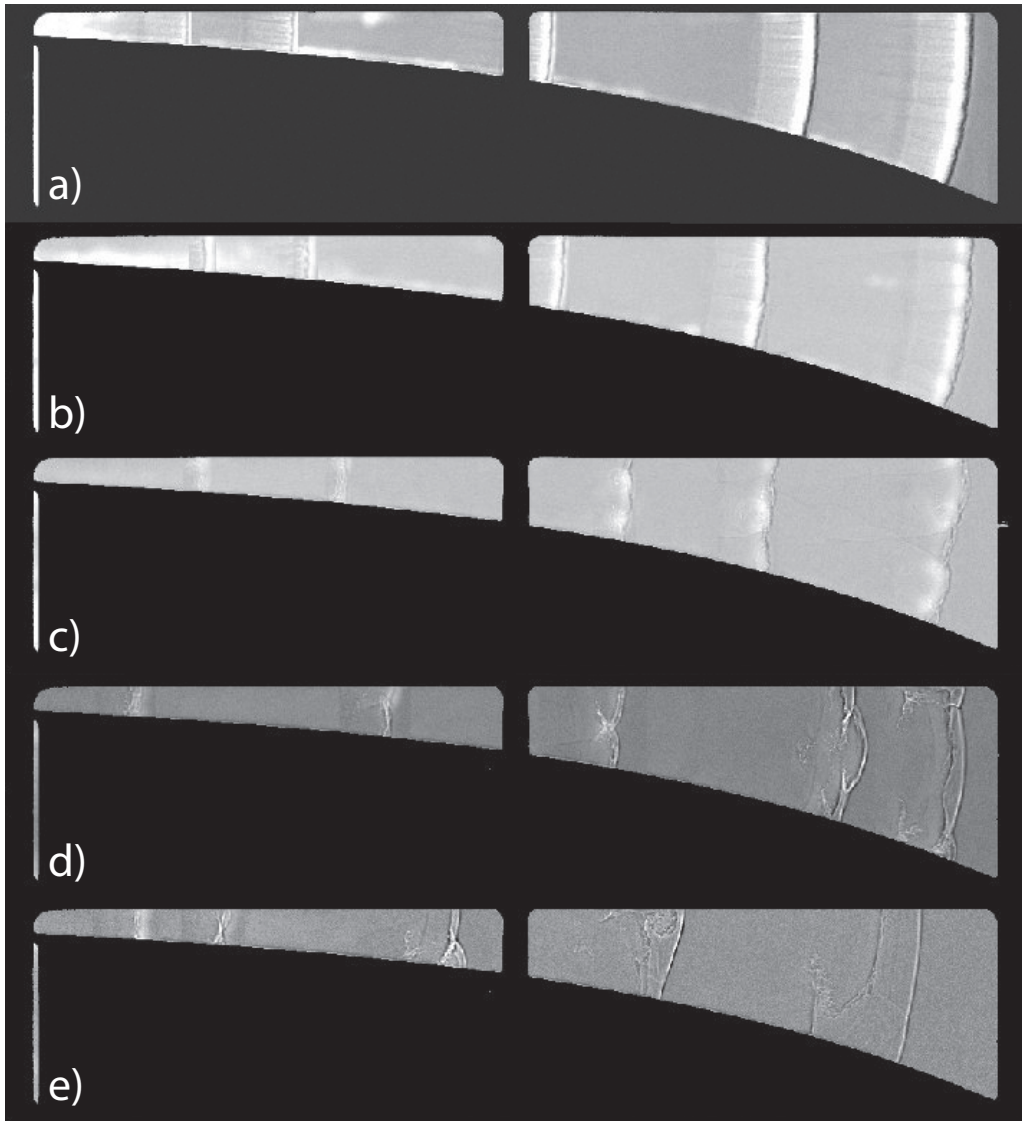


FIGURE 7. Detonation front evolution in $\text{C}_3\text{H}_8+5\text{O}_2$ along the long ramp at initial pressures of (a) 12.1 kPa, (b) 8.7 kPa, (c) 5.2 kPa, (d) 3.4 kPa and (e) 2.8 kPa.

4. Steady traveling wave solution

4.1. General formulation

We can now turn to the current models that predict the steady travelling wave detonation solution in the presence of lateral mass divergence. Numerous studies have addressed this in the past in the context of detonations with frontal curvature (Wood & Kirkwood 1954; Klein *et al.* 1995; Yao & Stewart 1995; Bdzil & Stewart 2007; He & Clavin 1994; Kasimov & Stewart 2005; Short & Bdzil 2003). Our treatment is however somewhat different, since the lateral mass divergence that is constant is the term K , the logarithmic derivative of the stream tube A in the laboratory frame of reference, given by (2.14), since this is what is kept constant in the experiments.

A physically relevant derivation starts with the governing equations for quasi-1D

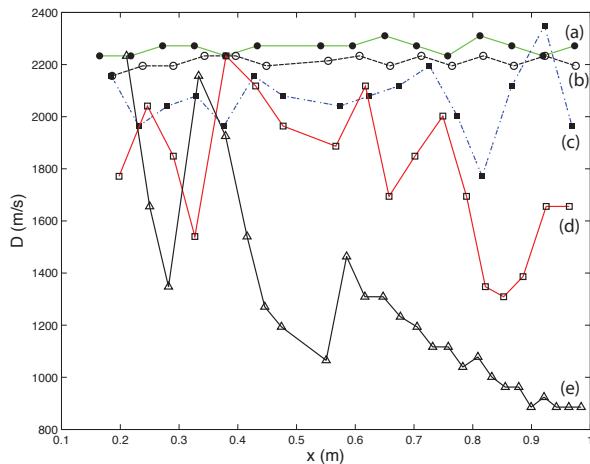


FIGURE 8. Speed of detonation front recorded along the top wall in $C_3H_8+5O_2$ along the long ramp at initial pressures of (a) 12.1 kPa, (b) 8.7 kPa, (c) 5.2 kPa, (d) 3.4 kPa and (e) 2.8 kPa, corresponding to the experiments shown in Fig. 7.

gasdynamics written in characteristic form (2.8). Seeking a travelling wave solution with speed D , we change to a wave-fixed frame with the change of variables $x' = Dt - x$, $t' = t$ and $v = D - u$ and requiring that the unsteady terms vanish (for the steady travelling wave), the differential operators transform as

$$\frac{D_{\pm}}{Dt} = (v \mp c) \frac{d}{dx'} \quad (4.1)$$

$$\frac{D}{Dt} = v \frac{d}{dx'} \quad (4.2)$$

With this transformation, the characteristic equation (2.9) becomes:

$$\frac{1}{\rho c^2} \frac{dp}{dx'} \mp \frac{1}{c} \frac{dv}{dx'} = \frac{\dot{\sigma} - \dot{\sigma}_A}{v \mp c} \quad (4.3)$$

with the upper and lower signs for the C_+ and C_- families of characteristics, respectively. Solving for the derivatives, we obtain the usual relations for the steady ZND structure of detonations:

$$\frac{dv}{dx'} = -\frac{1}{\rho v} \frac{dp}{dx'} = \frac{\dot{\sigma} - \dot{\sigma}_A}{1 - M^2} \quad (4.4)$$

with a similar expression for the density derivative:

$$\frac{d\rho}{dx'} = -\frac{\rho}{v} \left(\frac{dv}{dx'} + \dot{\sigma}_A \right) \quad (4.5)$$

With the appropriate kinetics to close the thermicity via (2.10) or (2.13), the structure of the travelling wave solution is readily obtained by integrating (4.4) and (4.5) from the shock at $x' = 0$. For a given shock speed D , the post shock state where the integration starts is given by the usual shock jump relations. The flow begins subsonic, but tends to increase its speed v due to energy release (and decrease through the opposite effect from the lateral divergence). As the flow may eventually become sonic, hence gasdynamically isolating the reaction zone from the rear flow, singular behaviour (marking non-steady dynamics) in (4.3), (4.5) and (4.4) is only prevented by the local balance between the thermicity $\dot{\sigma}$ and the rate of lateral strain $\dot{\sigma}_A$. This is the so-called generalized Chapman-

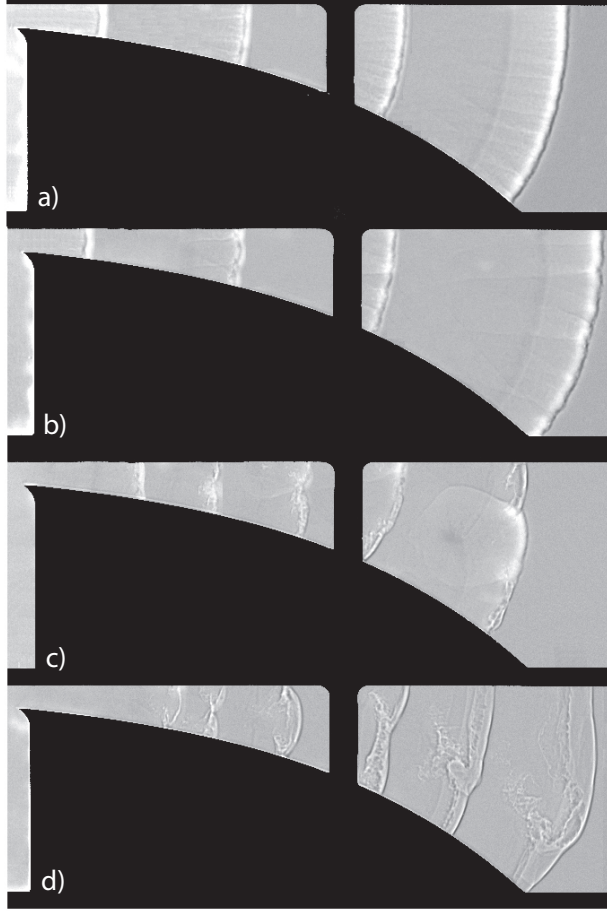


FIGURE 9. Detonation front evolution in $\text{C}_3\text{H}_8+5\text{O}_2$ along the long ramp at initial pressures of (a) 12.1 kPa, (b) 8.6 kPa, (c) 5.5 kPa, and (d) 4.5 kPa.

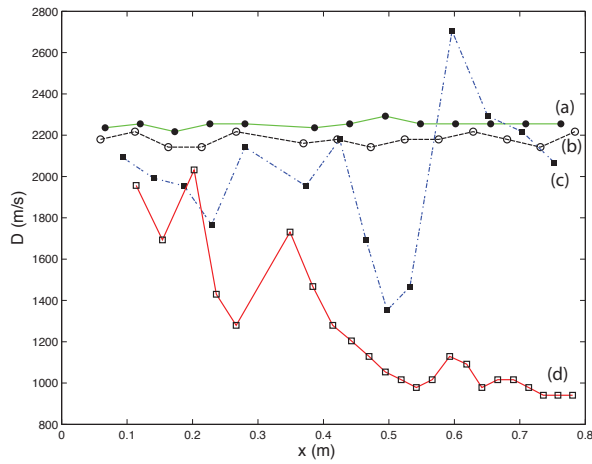


FIGURE 10. Speed of detonation front recorded along the top wall in $\text{C}_3\text{H}_8+5\text{O}_2$ along the shorter ramp at initial pressures of (a) 12.1 kPa, (b) 8.6 kPa, (c) 5.5 kPa, and (d) 4.5 kPa, corresponding to the experiments shown in Fig. 9.

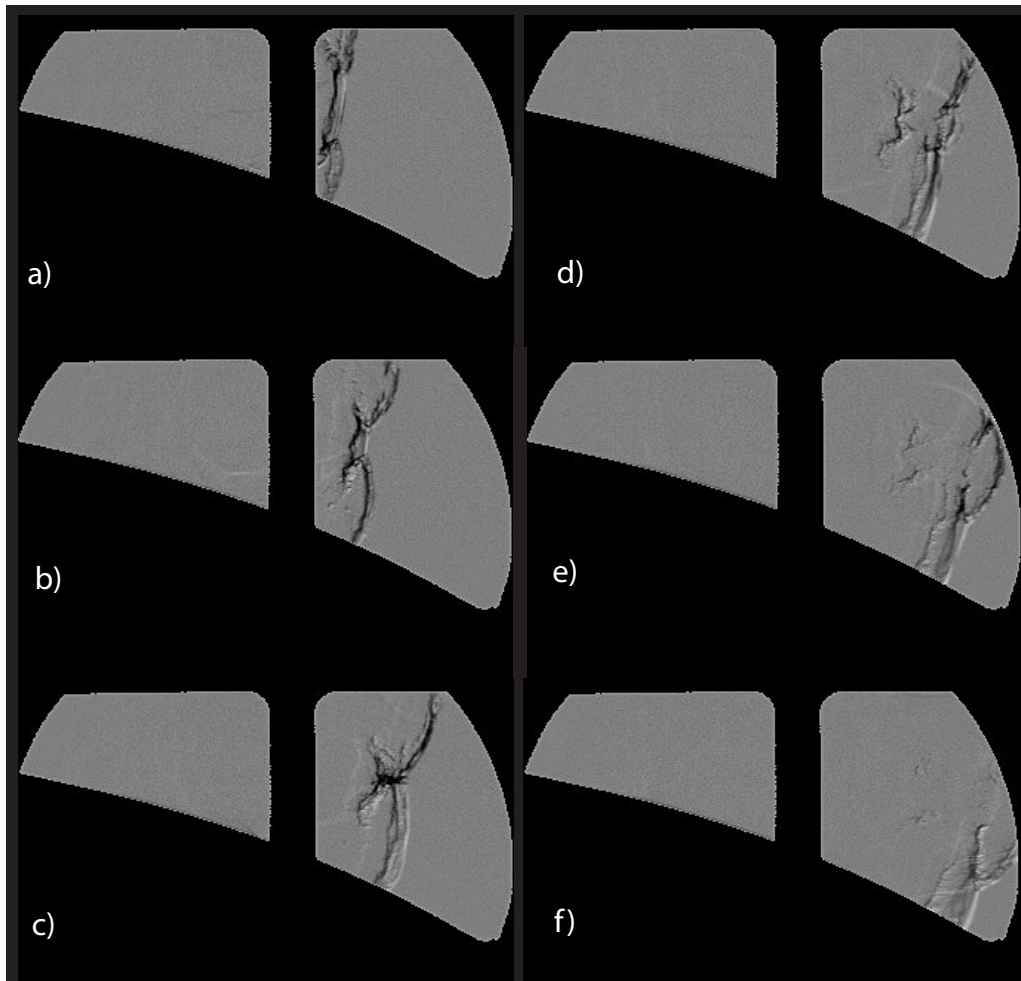


FIGURE 11. Sequence of Schlieren records illustrating the front evolution in $\text{C}_3\text{H}_8+5\text{O}_2$ along the short ramp at 4.5 kPa.

Jouguet criterion. This condition provides the rear boundary condition. The particular values of detonation speed that yield post-shock flows which will satisfy the generalized CJ condition somewhere in the reaction zone behind the lead shock will mark the possible steady state travelling wave solutions. Note that an interesting interpretation of this criterion can be physically interpreted by invoking the characteristic structure given by (4.3): the reaction zone structure can be seen to consist of a region where forward facing characteristic communicate pressure wave amplification forward to sustain the lead shock, while the limiting characteristic travels at precisely the lead shock speed, along which the vanishing of the overall thermicity ensures that the waves travelling forward are not amplified.

4.2. The kinetic model

In order to solve equations (4.5) and (4.4), a chemical kinetic model is required to establish the link between the evolution of each specie and the thermicity $\dot{\sigma}$ given by (2.10). While such calculations have been reported in the literature using complex kinetic schemes (Klein *et al.* 1995; He & Clavin 1994; Radulescu 2003; Chao *et al.* 2009; Camargo

et al. 2010; Gao *et al.* 2016), in the present study, we attempt to first reduce such kinetic descriptions to a much simpler two-step formulation, such that the same kinetic model can be applied to unsteady multi-dimensional simulations as well. Such calculations with detailed chemical models are computationally prohibitive.

Recently, systematic methods of replacing the full set of chemical reactions by a reduced reaction set have resulted in development of two-step induction-reaction models to represent these two phases of combustion. An early example of using a two-step reaction model is the work of Korobeinikov *et al.* (1972). Two-step models for reaction, have been used successfully in numerical simulations to reproduce observed characteristics of detonations and their structure in various problems. Some examples include the work of Oran *et al.* (1981), Taki & Fujiwara (1981), He & Clavin (1992), Oran *et al.* (1992) and Kailasanath *et al.* (1991). Therefore, in the current work, in order to avoid the difficulties and drawbacks of performing the detonation simulations with full chemistry, the two-step reaction model used by Short & Sharpe (2003) is adopted with the following equations for the induction and reaction progress variables. Solutions to curved detonations satisfying the generalized CJ condition have been discussed by Short & Bdzil (2003).

$$\frac{D\lambda_i}{Dt} = -K_i H(\lambda_i) e^{-\frac{E_a}{RT}} \quad (4.6)$$

$$\frac{D\lambda_r}{Dt} = K_r (1 - H(\lambda_i))(1 - \lambda_r) \quad (4.7)$$

In the above set of equations, λ_i denotes a progress variable for the induction zone, with a value of 1 in reactants and 0 at the end of the induction zone. K_i is a rate constant and $H()$ is the Heaviside function which turns off the rate of λ_i at the end of the induction zone. Likewise K_r and λ_r are the reaction zone rate constant and its progress variable respectively. The reaction zone progress variable λ_r is 0 in the induction zone and asymptotes to a value of 1 in the burned products. It is equivalent to the mass fraction of products, formally replacing Y_p in (2.4) and (2.5). This two-step model is used in the framework of a simple reactive perfect gas model, for which the equation of state is given by (2.4) and the thermicity is given by (2.13). The model has thus two thermodynamic constants to fit: the isentropic exponent γ and the heat release Q . It also has three kinetic parameters to fit: the activation energy E_a and the reaction constants K_i and K_r .

While there are numerous methods that can be used to extract meaningful values for detonation kinetic parameters in the framework of the reaction model chosen (Radulescu 2003; Liang *et al.* 2007; Browne *et al.* 2006; Borzou & Radulescu 2013), the present work adopts the method used by Radulescu (2003); Borzou & Radulescu (2013); Borzou (2016). In this method, the isentropic exponent γ was chosen to match the value obtained using realistic thermo-chemical data behind the lead shock propagating at the CJ speed, in order to correctly recover the gas compressibility in the reaction zone of detonations. The heat release Q was chosen such that the detonation Mach number that can be calculated using the perfect gas model (Lee 2008) matched the calculation result using the exact thermo-chemical data for that particular mixture.

The kinetic parameters were obtained by matching the induction and reaction times of the mixture at constant volume, taking the post shock conditions of the steady ZND structure in the absence of losses as initial state (the Von Neumann state). Fig. 12 shows the variation of the induction and reaction times with the initial pressure for both mixtures studied. The constant volume calculations were performed using the CANTERA package (Goodwin 2009). The Sandiego mechanism was used for the calculations in both mixtures, as it has been previously been shown to reproduce well experimental ignition

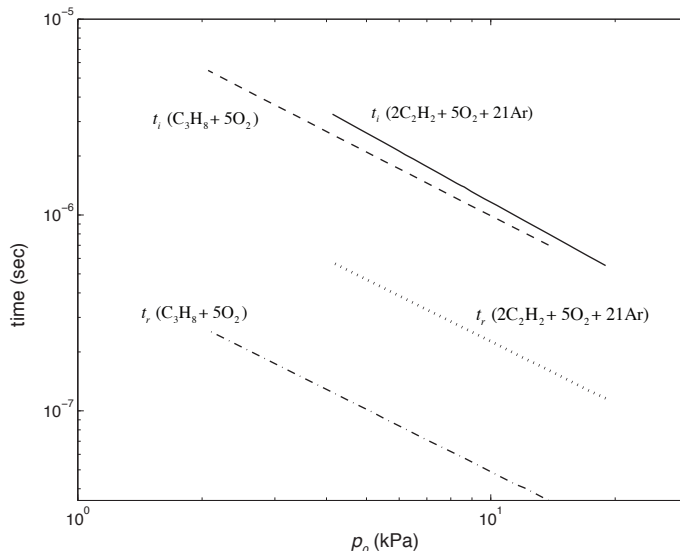


FIGURE 12. Variation of the ignition delay time $t_{i,N}$ and reaction time $t_{r,N}$ for the two mixtures with initial pressure calculated at the post shock conditions of the steady ZND structure in the absence of losses.

delay times in these two mixtures (<http://combustion.ucsd.edu>). Both mixtures have approximately the same ignition delay, although the propane mixture has a reaction time shorter than the diluted acetylene mixture by a factor of 5. All time scales vary approximately as an inverse power law with pressure.

Because all the relevant time scales varied in the same proportion with the initial pressure in the mixture, it is sufficient to tune the kinetic parameters at one particular reference pressure. The parameters were extracted for an initial pressure of 8.6 kPa and 300 K initial state for the acetylene mixture and 12.1 kPa initial pressure and 300 K for the propane mixture. The activation energy was extracted from the assumed dependence of the ignition delay $t_i = K_i^{-1} \exp\left(\frac{E_a}{RT}\right)$ obtained from (4.6) on initial temperature at the corresponding post shock thermodynamic state:

$$\frac{E_a}{RT_N} = \frac{1}{T_N} \left(\frac{d \ln t_i}{d(1/T)} \right)_{T=T_N} \quad (4.8)$$

The derivative was estimated numerically using the Cantera calculations by bracketing the Von Neumann state by 100 K. The parameters of the two-step reaction model extracted for both acetylene and propane mixtures using this method are reported in table 1. These are reported non-dimensionally, using the initial pressure p_0 as pressure scale, the initial density ρ_0 as characteristic density and the ZND induction length $\Delta_i = v_N t_i$ as characteristic length scale. In this manner, the same model can be used by appropriately re-scaling the two constant K_i and K_r for different initial pressures, where all the ignition times scales vary in the same proportion, as indicated in Fig. 12.

The two-step model fit is thus designed to recover the correct ignition delay variation with pressure, the correct ratios of reaction to induction times, and the correct dependence of ignition delay on temperature variations. For further comparison purposes, the two-step model was tested against the full chemistry in its prediction of the ZND profile in the absence of losses. Fig. 13 shows the pressure and density profiles behind a steady

TABLE 1. Kinetic parameters for the two-step model (4.6) and (4.7).

Mixture	γ	$\frac{E_a}{RT_0}$	$\frac{Q}{RT_0}$	$\frac{K_i \Delta_i}{\sqrt{RT_0}}$	$\frac{K_r \Delta_i}{\sqrt{RT_0}}$
$2C_2H_2+5O_2+21Ar$	1.42	27.8	18.3	86.1	8.13
$C_3H_8+5O_2$	1.14	56	99	8.47×10^4	5.13

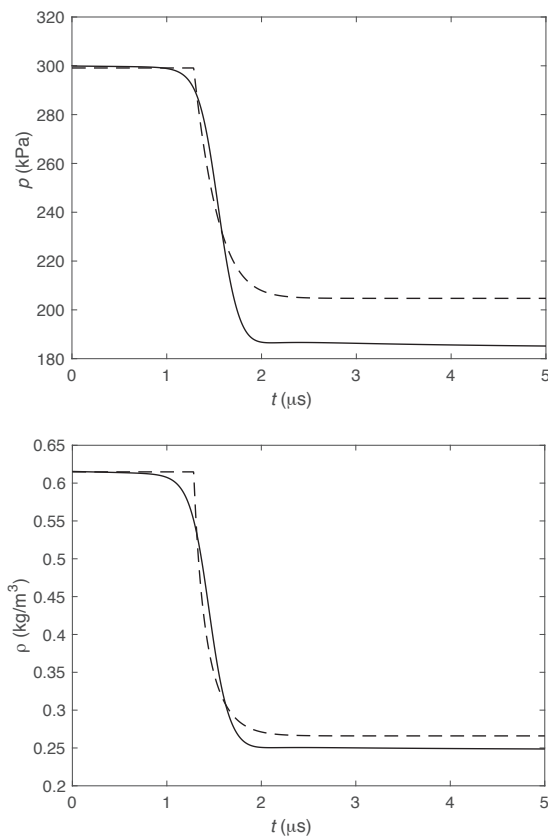


FIGURE 13. Pressure (top) and density (bottom) ZND profiles obtained with the Sandiego kinetic mechanism (full lines) and with the reduced two-step mechanism (broken lines) in $2C_2H_2+5O_2+21Ar$ at 8.6 kPa initial pressure.

detonation wave in $2C_2H_2+5O_2+21Ar$ at 8.6 kPa initial pressure. The profiles with the full chemistry were obtained by using the Shock and Detonation Toolbox developed by Shepherd and his students (Kao & Shepherd 2008). It can be seen that the ZND structure predicted by the two-step model is in good agreement with the full chemistry model. Note however that the burned gas state is not exactly recovered, since the perfect gas reactive model was calibrated only for the Mach number of the front and correct compressibility of the shocked gases.

4.3. Solutions

Adopting the kinetic model given by (4.6) and (4.7) to evaluate the thermicity in (2.13), the structure of the steady detonation with lateral mass divergence was obtained by integrating (4.5) and (4.4) from the shock, where the usual shock jump equations for a perfect gas apply, given the shock speed D . Hence, for a given value of D , a shooting procedure was used to determine the value of lateral mass divergence K that satisfied the generalized CJ criterion within the reaction zone.

The shooting procedure is as follows. First D was fixed. Starting with a sufficiently large value of K such that the flow could not reach the sonic condition anywhere, the value of K was lowered until the flow could reach the sonic condition. The largest value of K for a given D that permitted to have sonic flow ensured that the generalized CJ condition was also satisfied (Klein *et al.* 1995; He & Clavin 1994; Yao & Stewart 1995). This maximization, as well as the numerical integration of the ODE's, was performed numerically with Mathematica to within machine precision for the value of K . In this manner, the characteristic curves $K(D)$ can be constructed.

The calculations were performed using the parameters obtained from kinetic calculations for each mixture (see table 1). The results of the calculations for both acetylene-oxygen-argon and propane-oxygen mixtures are shown in Fig. 14. In this figure, the detonation speed normalized by the CJ speed is plotted with respect to the area divergence rate of the channel, normalized by the induction length. It can be seen that when the value of the area divergence is zero, the detonation is propagating with the CJ velocity as expected. For both mixtures, by increasing the value of the area divergence K , the corresponding velocity deficit for the shock increases until the curve reaches an inflection point where the detonation wave extinguishes. Further increase in the area divergence does not allow a steady state solution. The reason for this is the inability for the weaker thermicity to drive the flow to the sonic condition, as the flow divergence, having the opposite effect, is stronger. It can be seen that the critical rate of area divergence required for the extinction of the detonation wave is larger in the acetylene mixture. Also the critical velocity deficit in the acetylene mixture ($\simeq 14\%$) is more substantial than in propane mixture ($\simeq 6\%$), as expected from the much smaller activation energy in the acetylene system (Short & Bdzil 2003). Comparison with the experimental data is delayed until section 6.

5. Numerical Simulations of Cellular Detonations

In this section, we report the results of two-dimensional unsteady calculations of detonations propagating in a diverging channel. The calculations were only performed for the acetylene system using the reactive Euler equations and the parameters listed in Table 1. These have not been performed for the parameters corresponding to the propane experiments, due to the prohibitive computational overhead. This is primarily due to the significantly higher activation energy (see table 1), which would require much finer resolutions of positive temperature fluctuations, for which the rates are much faster. Likewise, as shown in Fig. 12, the reaction times in this mixture are approximately 5 times shorter than for the acetylene mixture, hence requiring an appropriately finer resolution. Furthermore, the experiments have revealed that diffusive phenomena control the burn-out of unreacted pockets, which hence requires appropriate closure of the transport terms and possibly turbulence modelling, as was recently attempted by Maxwell (2016) - the results of such calculations will be communicated in the near future.

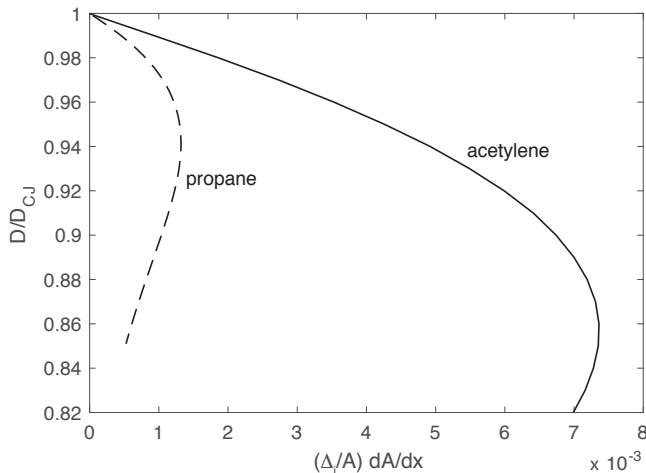


FIGURE 14. $D - K$ curves for quasi-one-dimensional detonations with mass divergence in the acetylene and propane mixtures.

5.1. Set-up

The numerical integration of the governing equations (2.1-2.3) for two dimensional flows was obtained using the MG code developed by S. Falle of the University of Leeds (Falle 1991; Falle & Komissarov 1991). The convective terms were evaluated using the exact Godunov scheme. The time evolution of the chemical source terms was performed explicitly and coupled to the hydrodynamics by the method of fractional time steps (Falle 1991). The code also features adaptive mesh refinement controlled by user defined differences between the solutions computed at different grid levels. In this regard, a hierarchical series of rectangular Cartesian grids $G^0 \dots G^n$ are used, so that grid G^n has the mesh spacing $h/2^n$ where h is the coarse grid size. The advanced solution on the grids G^{n-1} and G^n are compared on a cell by cell basis, to decide whether cells on the latter need to be refined. In the simulations, the base grid corresponded to one induction length Δ_i of the nominal detonation, while the subsequent finer grids offered finer resolutions.

The numerical domain consisted of a constant area duct further connected to a channel with a diverging cross-sectional area (see, for example, Fig. 15). The length and the height of the domain were 1000 and 100 induction zone lengths respectively. The length and the height of the constant area zone were 400 and 10 induction zone lengths respectively. Similar to the experiments performed in section 3, the diverging section of the domain had a cross-sectional area (height) varying exponentially.

All the solid surfaces were treated by a symmetry boundary condition. The curved wall was implemented directly on the Cartesian grid in a staircase fashion, using a symmetry boundary condition on each cell surface representing a gas-solid interface. This appeared as adequate when a sufficiently high resolution was used, as described below.

As initial conditions, a planar blast wave originating from a plane source of energy was prescribed at the beginning of the constant area zone. The energy source was a $1\Delta_i$ -thin band of the gas with the high pressure of $1000 p_0$ and ambient density ρ_0 . The decay of the ensuing blast wave initiated a detonation wave, which acquired its cellular structure via its own instability. The location of the start of the diverging ramp was determined by requiring that both the cellular structure and detonation speed became stationary.

The dynamics of the detonation wave were investigated in the diverging sections for

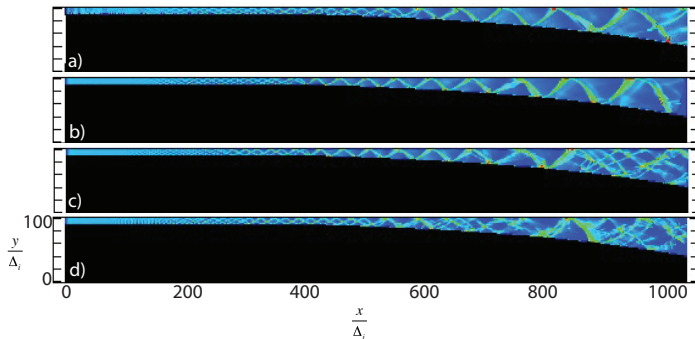


FIGURE 15. The open shutter images for $K\Delta_i=0.003$ obtained at resolutions with (a) 8, (b) 16, (c) 32, (d) 64 grid points per induction zone length Δ_i .

different divergence rates $K\Delta_i$, as this parameter controls the losses, as shown in Section 4. This is equivalent to changing the sensitivity of the mixture by varying its initial pressure in the experiments and hence the ignition length Δ_i and the reaction zone length.

5.2. Resolution and grid convergence

A grid convergence study was performed in order to determine the appropriate mesh refinement required to resolve correctly the detonation dynamics. The characteristic features of the cellular structure obtained for the detonation wave and mean speed of the detonation front were compared at these different resolutions. This study was performed for the divergence rate of $K\Delta_i = 0.003$. Simulations were run with 3, 4, 5 and 6 levels of refinement in the most refined grid corresponding to 8, 16, 32 and 64 grids per induction zone length of the non-attenuated detonation, respectively.

Fig. 15 shows the numerical open shutter images taken by tracking the maximum thermicity. The records illustrate the time history of the cellular instabilities for the detonation front, as the maximum thermicity is associated with the gases behind the transverse waves (Lee 2008). The results obtained for all simulations showed qualitatively similar results. Before entering the diverging section, a double headed detonation is established. In the diverging section, the front re-organizes into a single large cellular structure with spontaneous re-appearance of cells. The higher resolutions of 32 and 64 grid points per induction length of the non-attenuated detonation recover approximately the same type of events of the birth of new cells after sufficiently large cells are formed, as occurring at $x/\Delta_i=800$. Note that as the single headed detonation attenuated by the diverging section becomes essentially better resolved than the nominal un-attenuated detonation in the straight duct, owing to its larger reaction zone structure for the same physical resolution.

A more quantitative comparison can be drawn by comparing the mean detonation speed obtained at each resolution, since this is a direct measure of the mean thermicity in the reaction zone (according to the discussion of the mean structure of sections 2 and 4). Table 2 shows the average speed of the detonation front measured along the top wall of the diverging domain for the resolutions using 8, 16, 32 and 64 grid points per induction length Δ_i . It can be seen that the results obtained for the 32 and 64 grid points are converged to within 1%, which is comparable with the precision of the experimental measurements shown in Fig. 6.

The convergence study performed showed that five refinement levels corresponding to

TABLE 2. Time averaged speed of the detonation wave measured along the top wall of the domain for an area divergence of $K\Delta_i=0.003$ at different levels of grid resolution.

Grid points per induction length Δ_i	D/D_{CJ}
8	0.93
16	0.94
32	0.92
64	0.92

the resolution of 32 grids per induction zone of the non-attenuated detonation permitted to obtain grid-converged solutions for the acetylene mixture. Based on the above qualitative and quantitative observations about the solutions at different resolutions, the resolution of 32 grids per induction zone length was adopted for the study.

5.3. Results

Fig. 16 shows the integrated maximum thermicity field in channels with non-dimensional divergence rate $K\Delta_i$ of 0.002, 0.003, 0.004, 0.005 and 0.006. Fig. 17 shows the same evolution of the detonation wave fronts by superposing five records of the density gradient field (pseudo-Schlieren image) at five sequential times. Fig. 18 shows the speeds of the lead shock recorded along the top wall for the calculations corresponding to $K\Delta_i$ of 0.002, 0.004 and 0.006.

At a divergence of $K\Delta_i$ of 0.002, the detonation structure in the diverging section corresponds to single mode propagation, with the onset of multiple modes occurring only at the end of the channel, when the domain width has approximately doubled. The reaction zone structure of this detonation front is in general good agreement with experiment, in that transverse waves with closely coupled reactivity are generally observed, without significant formation of separated pockets.

At larger divergence rates of the channel cross-section $K\Delta_i$ of 0.004, the reaction zone is thicker. The onset of new cells occurs again when the width of the channel has approximately doubled at $x \simeq 700$. The enlarged cells, however, seem to depart from the reactive transverse wave configuration observed in the experiments. Instead, larger non-reacted pockets are seen to detach from the front, as can be seen in the various frames of Fig. 17.

While at $K\Delta_i$ of 0.005, a detonation was observed to propagate the length of the diverging channel, an increase of the divergence to 0.006 resulted in the detonation failing in the diverging channel, as shown in Figs. 16(e), 17(e) and 18(e). As the cellular structure disappeared, the detonation front separated into a lead shock and contact surface. Note the thinning out of the reactive pockets by some numerical diffusion in Fig. 17(e).

6. Discussions

We can now draw several conclusions by comparing the $D - K$ curves obtained experimentally, numerically in two-dimensional unsteady simulations and the steady wave prediction.

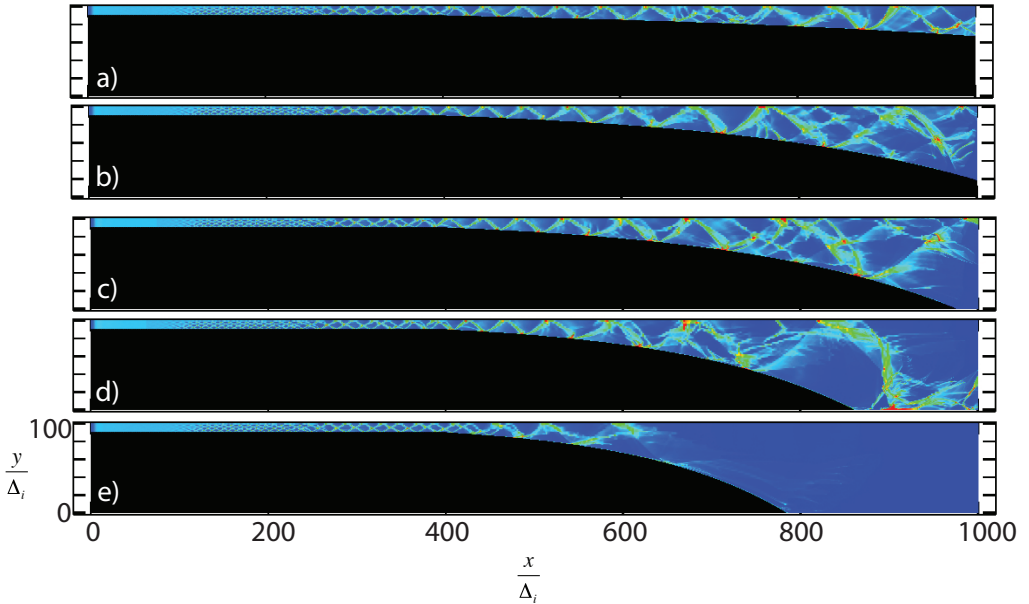


FIGURE 16. The evolution of the detonation wave structure, visualized by tracking the maxima in the thermicity at each location for $K\Delta_i$ of 0.002 (a), 0.003 (b), 0.004 (c), 0.005 (d) and 0.006 (e).

6.1. Comparison between inviscid cellular simulations and steady travelling wave prediction.

The first comparison is between the cellular simulation results of Section 5 and the steady travelling wave prediction of Section 4. Fig. 19 shows the mean detonation speed obtained in the unsteady simulations and the one-dimensional steady travelling wave solution for the same parameter set. As can be seen, the detonation speed obtained in the cellular simulations is *lower* than the speed of the steady travelling wave for the same stream tube divergence. Also, the critical value of area divergence that suppresses the detonation propagation is *smaller* in the unsteady simulations. These observations indicate the role of an inviscid cellular instability on the propagation mechanism of detonations. The inviscid cellular instability appears to *weaken* the propagation mechanism of such detonations. This finding is in agreement with the observations of Radulescu *et al.* (2007a), who have determined the same trend in the problem of detonation initiation by a decaying blast. They had observed that a perturbed detonation in which a cellular instability was induced requires *more* energy for direct initiation than a 1D detonation devoid of instabilities. They rationalized this finding by observing that the reaction zone structure of a cellular detonation is thicker than the reaction structure of a 1D detonation. This is primarily due to the exponential sensitivity of the reaction rates to temperature. Material processed by weaker shocks skew the average reaction structure to much longer length scales as compared to the structure predicted by the ZND model (Radulescu *et al.* 2007b). The present result is also consistent with the results of Sow *et al.* (2014), who investigated the dynamics of one-dimensional pulsating detonations with friction and found that detonations undergoing a pulsating instability were more prone to failure than anticipated from the structure of the travelling wave solution (ZND model with friction). Similar results were also obtained by Mazaheri *et al.* (2015), when comparing the detonations with mass divergence in porous wall tubes in simulations, experiments and

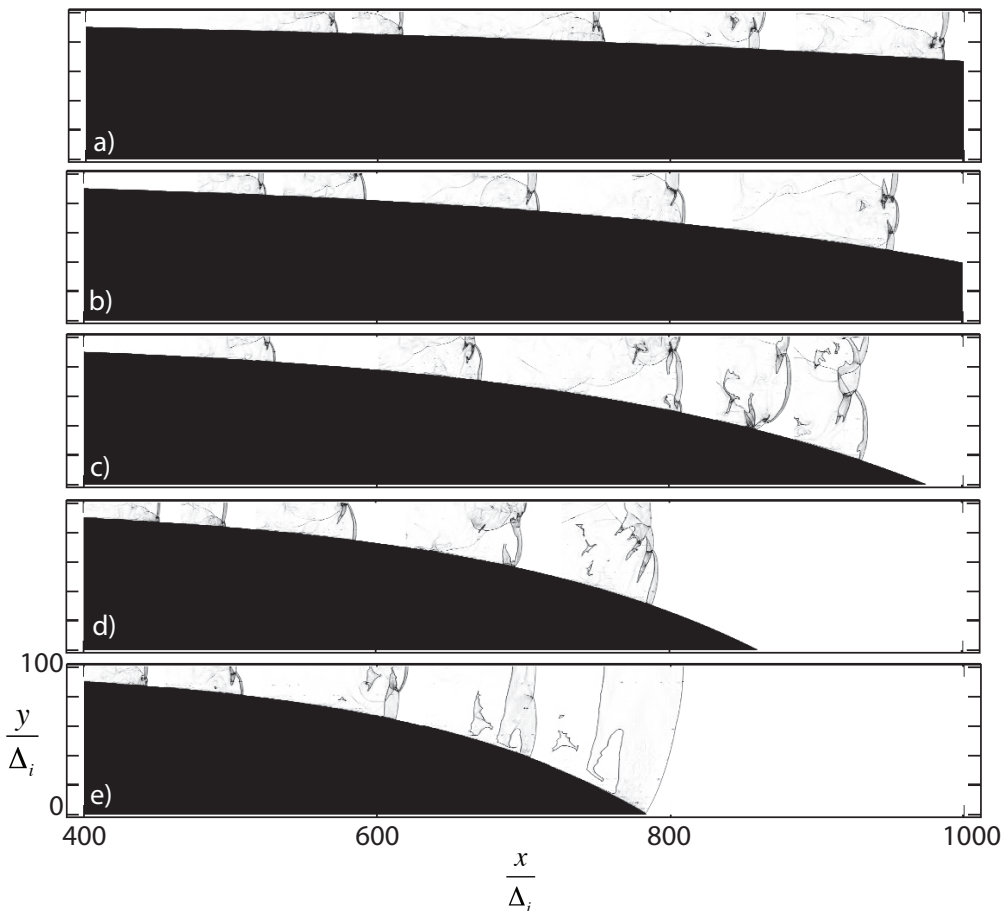


FIGURE 17. The evolution of the detonation wave structure, visualized by overlaying the density gradient fields at five discrete times in the diverging channel for $K\Delta_i$ of 0.002 (a), 0.003 (b), 0.004 (c), 0.005 (d) and 0.006 (e).

steady wave configurations. We can thus conclude that cellular detonations in the absence of diffusive processes, computed with the reactive Euler equations, may have narrower limits than predicted from steady state models. This finding is somewhat opposite to a long held idea that the inviscid detonation cellular structures play an important role in the propagation of detonations (Lundstorm & Oppenheim 1969). While this is an important finding of the current work, it remains to be verified with further calculations until a universal trend can be established.

6.2. Comparison with experiment.

We now turn to the comparison of the travelling wave ZND solution and unsteady simulations with the experimental results. The total mass divergence rate experienced by the detonation wave in the experiments of this study is due to the area divergence due to the diverging channel *and* the divergence of the flow to the boundary layers on the channel walls inherent in a thin channel geometry, by the mechanism discussed in Section 1. The effective lateral flow divergence rate thus includes both the contribution

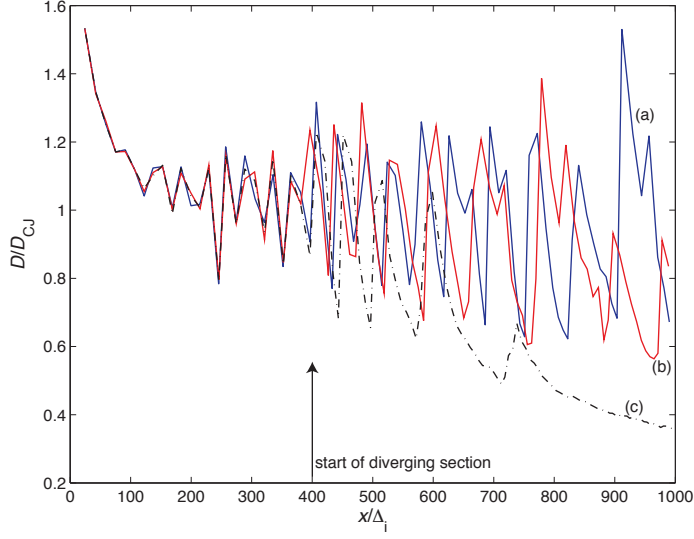


FIGURE 18. The speed of the lead shock along the top wall for diverging channels with a) $K = 0.002$, b) $K = 0.004$ and c) $K = 0.006$.

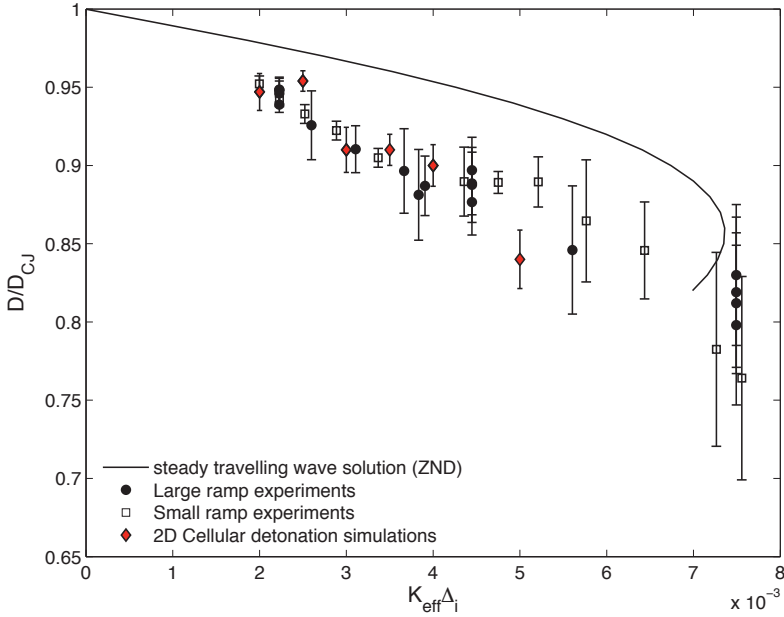


FIGURE 19. The $D - K$ characteristic curves for $2C_2H_2+5O_2+21Ar$ constructed using the experimental data, steady travelling wave ZND solution and unsteady two-dimensional calculations.

from the the diverging geometry and and the contribution of the flow divergence rate due to the boundary layers developing on the walls of the channel, ϕ_{BL} :

$$K_{eff} = \frac{1}{A} \frac{dA}{dx} + \phi_{BL} \quad (6.1)$$

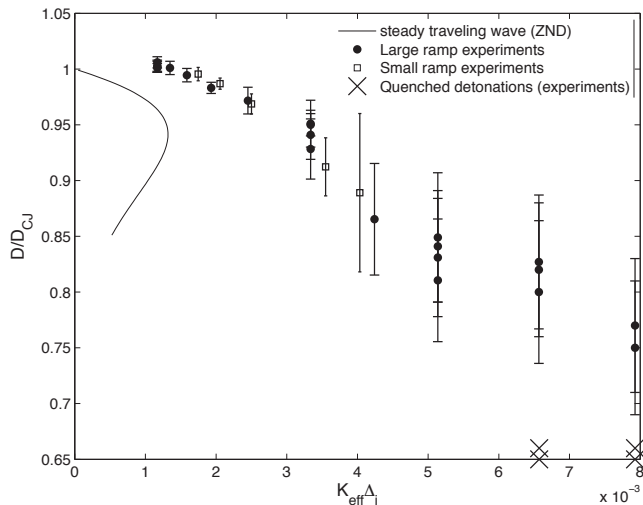


FIGURE 20. The $D - K$ characteristic curves for $C_3H_8+5O_2$ obtained experimentally and predicted from the quasi-one-dimensional ZND model using the chemical kinetic data of table 1.

Instead of modelling the source term ϕ_{BL} , which cannot be done without an empirical constant (Chao *et al.* 2009; Camargo *et al.* 2010; Gao *et al.* 2016), this loss rate can be directly evaluated from the experiments conducted on the two ramps of different expansion ratios, but constant channel dimension (19 mm), leading to a constant ϕ_{BL} . The contribution of the boundary layers losses ϕ_{BL} has been obtained experimentally by comparing the experiments performed on the two ramps, for the same mixture, and same velocity deficit and calibrating the effective rate of mass divergence K_{eff} to obtain a unique relation between velocity deficit and loss rate, as expected from theoretical considerations. Figs. 19 and 20 show the data obtained after such a reduction of the data shown in Fig. 6, using the kinetic calculations for the induction length derived from Fig. 12. It was found that a unique value of $\phi_{BL} = 5.5m^{-1}$ permitted to collapse all data for the two ramps in both mixtures tested.

Fig. 19 shows the comparison of $D - K$ curves obtained experimentally, numerically and the steady travelling wave ZND prediction. The cellular simulations are found in excellent agreement with experiment until approximately a divergence of $K\Delta_i = 0.005$. For a higher rate of divergence of 0.006, the calculations show that a detonation was cannot remain self-sustained. The experiments, however, showed that detonations with expansion rates larger by approximately a factor of $\simeq 1.4$ are possible. Perhaps coincidentally, the limit obtained in the experiments was however very well predicted by the steady travelling wave solution. The conclusion that can be drawn from the comparison with the experiments is that the inviscid cellular simulations capture very well the experimental results. The neglect of viscous terms and diffusion controlled burn-out of non-reacted pockets is warranted. The fact that the detonation in the experiments may propagate at slightly higher divergence rates and higher velocity deficits may be however due to many shortcomings of the modelling: three dimensional effects, chemical kinetic inaccuracies, and/or the inability of the numerical model to reproduce the transverse detonations observed in the experiments. These higher order effects will be investigated in the near future.

Also noteworthy is that the velocity deficit observed in the experimental curve of Fig.

19 for a given divergence rate does not agree with the prediction of the steady state model, where approximately twice the velocity deficit was observed in the experiments. Perhaps coincidentally however, the limit obtained in the experiments was however very well predicted by the steady travelling wave solution. Similar trends were reported by Radulescu & Lee (2002). This persisting trend calls for further scrutiny in other reactive mixtures and a rational justification.

Although no simulations were attempted for the more unstable detonation due to the requirement of properly addressing transport phenomena augmented by turbulence (Maxwell 2016), it is still worthwhile comparing the reduced experimental results with the steady travelling wave solution obtained in Section 4. For this much more unstable mixture, the departure between the experimental and steady solution is much more considerable, as can be seen in Fig. 20. First we observe the opposite trend of the acetylene mixture. The experimental curve indicates that for a given divergence rate, the velocity deficit is *smaller* in the experiments than predicted by the model. Likewise, we observe that detonations in the experiments may propagate at area divergences up to seven times larger than predicted by the steady model. While such discrepancies may be argued to be a signature of faulty kinetics, we do not think this is the reason. Incorrect predictions of kinetics time scales would only shift the prediction curve left or right, i.e., re-scale the abscissa, but would not affect the velocity deficits, which are a very strong function of the sensitivity of the kinetics, i.e., via the global activation energy. Instead, we believe that the large discrepancy between experiments and predictions is due to the burning mechanism in the highly-unstable detonations, which is not captured in the model. As shown in Fig. 11, layers of shocked, non-reacted gas reacts by diffusive processes (flames), consistent with the results of Maxwell (2016) and Radulescu *et al.* (2007b). This phenomenon is to reduce the thermal sensitivity of the global thermicity, as it is shown empirically below. A similar trend has been observed in previous such comparisons by Radulescu & Lee (2002); Radulescu (2003); Chao *et al.* (2009); Camargo *et al.* (2010); Mazaheri *et al.* (2015).

Another interesting observation of the experiments is the extrapolation of the detonation speed measured experimentally to zero divergence in Figs. 19 and 20. For the acetylene mixture, the experimental data appear to extrapolate well to the predicted CJ speed. For the more unstable detonations in propane, the experimental data extrapolate to speeds in excess of the CJ prediction by a few percent. This result is also compatible with previous measurements, which typically report propagation speeds, when extrapolated to zero losses, larger than the CJ predictions by a few percent - see Fickett & Davis (1979) for discussion and earlier references.

6.3. *Effective reaction models for cellular detonations.*

From a more practical perspective, the experimental technique developed in the present study of determining the detonation speed relation on the area divergence can be used to tune macroscopic models for the detonation dynamics, in a somewhat similar fashion to condensed phase reaction modelling. One of the simplest models that can be postulated is the two step model discussed earlier in Section 4, although now its parameters can represent the global behaviour of detonations at macro-scales. While not entirely satisfactory, as important physics are washed out, this purely empirical framework may be used, in the future for predictive purposes. It is nevertheless instructive to comment here on the magnitude of the fitting constants.

We have thus conducted this curve-fitting exercise, with the constraint that the induction length in the empirical model also be matched to that predicted by complex chemistry, such that the comparison be made on the basis of the non-dimensional terms

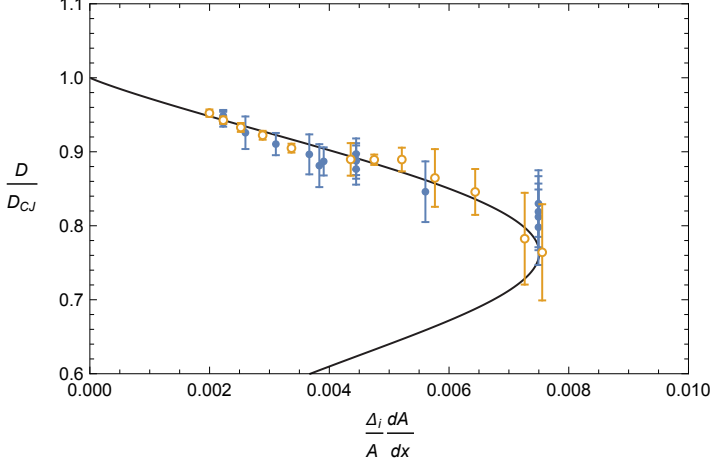


FIGURE 21. Fit of a $D - K$ curve to the experimental data obtained for the $2\text{C}_2\text{H}_2+5\text{O}_2+21\text{Ar}$ mixture in order to obtain the effective reaction rate parameters.

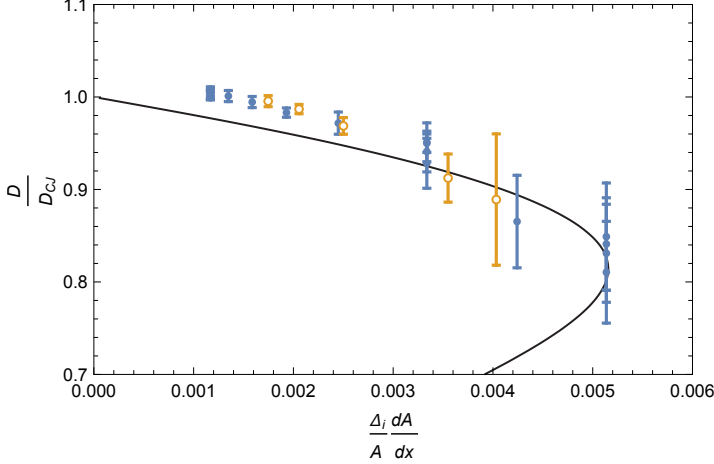


FIGURE 22. Fit of a $D - K$ curve to the experimental data obtained for the $\text{C}_3\text{H}_8+5\text{O}_2$ mixture in order to obtain the effective reaction rate parameters.

appearing in Figs. 19 and 20, and generalized to other operating conditions through simple scaling laws. As such, the only tuning parameters are the ratios of induction to reaction time, reflected by the ratio of reactions rate constants K_r/K_i , and the effective activation energy E_a . It was empirically verified that the fitting was single valued, although it can also be shown under some particular limits (Short & Bdzil 2003). The global activation energy controls mainly the velocity deficit attainable, while the induction to reaction time ratio controls the maximum amount of loss at the limit (Short & Bdzil 2003).

Curve-fits obtained by such a calibration yield the parameter set given in Table 3. The corresponding $D - K$ curves are shown in Figs. 21 and 22 for the two mixtures. A very good agreement can be obtained with experiment empirically for both mixtures. Nevertheless, the calibration also highlights what the effective activation energies are in these fits, as compared with those derived from the underlying chemistry, shown in Table 3. For the acetylene mixture, the reduction in effective activation energy is 26%, while

TABLE 3. Kinetic parameters for the two-step model obtained from fitting the $D - K$ curves to experiment.

Mixture	$\frac{E_a}{RT_0}$	$\frac{K_i \Delta_i}{\sqrt{RT_0}}$	$\frac{K_r \Delta_i}{\sqrt{RT_0}}$
$2C_2H_2+5O_2+21Ar$	20	1.1	27
$C_3H_8+5O_2$	16	5.6	19

for propane, the reduction in the activation energy is by 70%! The significantly lower effective activation energies, particularly for the much more unstable propane mixture, are not surprising, as it was already noted that the enhancement of burning mechanism in turbulent detonations by turbulent mixing suppresses much of the thermal character of the ignition mechanism, where the reaction zone length does not grow with velocity deficit, as anticipated from thermal ignition considerations (Radulescu *et al.* 2007b). Instead, the rapid burn-out of non-reacted pockets by diffusive processes explains why the reaction zones remain substantially shorter. In a global sense, the global reactions rate can be modelled with a lower activation energy. It is also noteworthy that Sow *et al.* (2014) also showed empirically that the effective activation energy in a pulsating detonation is lower than that for a steadily propagating wave. This highlights again that predictions made with the *steady* ZND model, using the kinetically derived rate constants for that particular fuel, are incorrect, and can lead to predictions departing from the experiments by approximately an order of magnitude in more unstable detonations.

7. Conclusion

The present work addressed the question of whether mean field macroscopic models are suitable to describe the dynamics of real cellular detonations in gases. This question was posed in the framework of detonations with stream-tube area divergence that is kept constant, as to generate attenuated detonations in steady state. The experiments have demonstrated that cellular detonations in both the weakly unstable ($2C_2H_2+5O_2+21Ar$) and strongly unstable mixture ($C_3H_8+5O_2$) had a constant propagation speed in the diverging section. This strongly suggests that a macroscopic mean field description is worthwhile for both weakly unstable and strongly unstable cellular gaseous detonations.

Three types of models were tested to describe these dynamics: empirical models tuned to the experiments, steady wave predictions based on the underlying chemistry and inviscid non-steady multi-dimensional simulations. From a purely empirical point of view, it was shown that effective reaction models can be tuned against such experiments. Future study should address the utility of such macroscopic models in predicting other dynamic phenomena of detonations, such as direct initiation or diffraction problems.

Secondly, unsteady cellular simulations of the inviscid reactive gasdynamic equations were performed for the $2C_2H_2+5O_2+21Ar$ system with a chemical kinetic model derived from the underlying multi-step chemical decomposition of this fuel. It was shown that the simulations were in excellent agreement with experiment for moderate divergence rates, but some minor discrepancies were observed near the limits. Overall, it can be concluded that inviscid type calculations can reproduce the experimental results correctly in this type of weakly unstable detonations.

The unsteady simulations also served to comment on the relevancy of the steady state models to capture unstable cellular detonation dynamics *for the same kinetic mechanism*. It was found that the cellular simulations of inviscid detonations lead to departures from the steady wave prediction. The unstable cellular simulations gave rise to larger velocity deficits at a given global divergence rate, as well as to a smaller maximum divergence rate. This comparison highlighted that inviscid cellular detonations may have narrower limits than predicted by steady models, confirming previous observations.

Finally, the experiments obtained in the much more unstable mixture $\text{C}_3\text{H}_8+5\text{O}_2$ showed that there were very large departures between the experimentally derived $D-K$ curve and the prediction of steady wave propagation based on the underlying chemistry. The reason for this discrepancy is likely to be due to the importance of diffusive processes in the burn-out of the the non-reacted pockets during the propagation, as observed from the reaction zone visualization. Furthermore, the empirical tuning of a global induction-reaction model to describe the experimental trends revealed that the effective activation energy was lower by 70% than the value derived from the real kinetics of the fuel decomposition. This supports the view that diffusive processes in highly unstable detonations may be responsible for reducing the thermal ignition character of the gases processed by the detonation front (Radulescu *et al.* 2007*b*).

We wish to acknowledge the NSERC Discovery Grant to MIR and partial support from the NSERC Hydrogen Canada (H2CAN) Strategic Research Network as well as Shell. We would like to acknowledge Professor Sam Falle of the University of Leeds for providing the numerical platform used in the study. We would also like to thank Karl German, Terrence R. Phenix, Mohammed Saif Al Islam and Qiang Xiao for help in conducting the experiments and Gary Sharpe for useful discussions. The insightful comments provided by the PhD committee of BB, comprising Gaby Ciccarelli, John Gaydos, Catherine Mavriplis and James McDonald are also greatly acknowledged. MIR dedicates this paper to Bambaleo and Ugobugo.

REFERENCES

- ARIENTI, M. & SHEPHERD, J. E. 2005 A numerical study of detonation diffraction. *Journal of Fluid Mechanics* **529**, 117–146.
- AUSTIN, J 2003 The role of instability in gaseous detonation. PhD thesis, California Institute of Technology, Pasadena, California.
- BDZIL, J B & STEWART, D S 2007 The dynamics of detonation in explosive systems. *Ann. Rev. Fluid Mech.* **39**, 263–292.
- BHATTACHARJEE, R 2013 *Experimental investigation of detonation re-initiation mechanisms following a mach reflection of a quenched detonation*. M.Sc Thesis, Department of Mechanical Engineering, University of Ottawa, Ottawa, ON.
- BORZOU, B 2016 The influence of cellular structure on the dynamics of detonations with constant mass divergence. PhD thesis, University of Ottawa, Ottawa, ON.
- BORZOU, B & RADULESCU, M I 2013 *Evaluation of hydrogen, propane and methane-air detonations Instability and detonability*. Brussels, Belgium: International Conference on Hydrogen Safety, ICHS.
- BROWNE, S, ZEIGLER, J & SHEPHERD, J E 2006 Numerical solution methods for shock and detonation jump conditions. *GALCIT Technical Report FM2006.006*.
- CAMARGO, A, NG, H D, CHAO, J & LEE, J H S 2010 Propagation of near-limit gaseous detonations in small diameter tubes. *Shock Waves* **20**, 499–508.
- CHAO, J, NG, H D & LEE, J H S 2009 Detonability limits in thin annular channels. *Proc. Combust. Inst.* **32**, 2349–2354.
- CHINNAYYA, A, HADJADJ, A & NGOMO, D 2013 Computational study of detonation wave propagation in narrow channels. *Phys. Fluids* **25**, 036101.

- DABORA, E K, NICHOLLS, J A & MORRISON, R B 1965 The influence of a compressible boundary on the propagation of gaseous detonations. *Proc. Combust. Inst.* **10**, 817.
- DEITERDING, R 2003 Parallel adaptive simulation of multi-dimensional detonation structures. PhD thesis, Brandenburgischen Technischen Universität Cottbus, Cottbus, Germany.
- DENNIS, K, MALEY, L, LIANG, Z & RADULESCU, M I 2014 Implementation of large scale shadowgraphy in hydrogen explosion phenomena. *International Journal of Hydrogen Energy* **39**(21), 11346–11353.
- DUPRE, G, PERALDI, O, LEE, J H S & KNYSTAUTAS, R 1991 *Dynamics of detonations and explosions: Detonations, Vol(133), Chapter: Limit criterion of detonation in circular tubes*. University of Colorado at Boulder: Progress in astronautics and aeronautics.
- ECKETT, C A, QUIRK, J J & SHEPHERD, J E 2000 The role of unsteadiness in direct initiation of gaseous detonations. *J. Fluid Mech.* **421**, 147–183.
- EDWARDS, D. H., THOMAS, G. O. & NETTLETON, M. A. 1979 Diffraction of a planar detonation-wave at an abrupt area change. *Journal of Fluid Mechanics* **95** (NOV), 79–96.
- FALLE, S A E G 1991 Self-similar jets. *Mon. Not. R. astr. Soc.* **250**, 581–596.
- FALLE, S A E G & KOMISSAROV, S S 1991 An upwind numerical scheme for relativistic hydrodynamics with a general equation of state. *Mon. Not. R. astr. Soc.* **250**, 581–596.
- FAY, J A 1959 Two-dimensional gaseous detonations: velocity deficit. *Phys. Fluids* **2**, 283–289.
- FICKETT, W & DAVIS, W C 1979 *Detonation theory and experiment*. Dover Publication Inc.
- GAMEZO, V. N., VASIL'EV, A. A., KHOKHLOV, A. M. & ORAN, E. S. 2000 Fine cellular structures produced by marginal detonations. *Proceedings of the Combustion Institute* **28**, 611–617.
- GAO, Y., ZHANG, B., NG, H. D. & LEE, J. H. S. 2016 An experimental investigation of detonation limits in hydrogen-oxygen-argon mixtures. *International Journal of Hydrogen Energy* **41** (14), 6076–6083.
- GOODWIN, D 2009 An object-oriented software toolkit for chemical kinetics, thermodynamics, and transport processes. *Technical Report Caltech, Pasadena*.
- HE, L & CLAVIN, P 1992 Critical conditions for detonation initiation in cold gaseous mixtures by nonuniform hot pockets of reactive gas. *Proc. Combust. Inst.* **24**, 1861–1867.
- HE, L T & CLAVIN, P 1994 On the direct initiation of gaseous detonations by an energy source. *J. Fluid Mech.* **277**, 227–284.
- HU, X Y, ZHANG, D L, KHOO, B C & JIANG, Z L 2005 The structure and evolution of a two-dimensional H₂/O₂/Ar cellular detonation. *Shock Waves* **14**, 37–44.
- KAILASANATH, K, GARDNER, J H, BORIS, J P & ORAN, E S 1991 Numerical simulations of unsteady reactive flows in a combustion chamber. *Combust. Flame* **86**, 115–134.
- KAO, S. 2008 Detonation stability with reversible kinetics. PhD thesis, California Institute of Technology, Pasadena, California.
- KAO, S. & SHEPHERD, J.E. 2008 Numerical solution methods for control volume explosions and znd detonation structure. *Tech. Rep. GALCIT Report FM2006.007*. California Institute of Technology, Pasadena, California.
- KASIMOV, A. R. & STEWART, D. S. 2005 Asymptotic theory of evolution and failure of self-sustained detonations. *Journal of Fluid Mechanics* **525**, 161–192.
- KLEIN, R, KROK, J C & SHEPHERD, J E 1995 Curved quasi-steady detonations: Asymptotic analysis and detailed chemical kinetics. *GALCIT Report FM 95-04*.
- KOROBENIKOV, V P, LEVIN, V A, MARKOV, V V & CHERNYI, G G 1972 Propagation of blast waves in a combustible gas. *J. Astronautica Acta* **17**, 529–537.
- LEE, J H S 1984 Dynamic parameters of gaseous detonations. *Ann. Rev. Fluid Mech.* **16**, 311–336.
- LEE, J H S 2008 *The Detonation Phenomenon*. Cambridge: Cambridge Univ. Press.
- LIANG, Z, BROWNE, S, DEITERDING, R & SHEPHERD, J E 2007 Detonation front structure and the competition for radicals. *Proc. Combust. Inst.* **31**, 2445–2453.
- LUNDSTORM, E A & OPPENHEIM, A K 1969 On the influence of non-steadiness on the thickness of the detonation wave. *Proc. Roy. Soc.* **310**, 463–478.
- MALEY, L 2015 *On shock reflections in fast flames*. M.Sc Thesis, Department of Mechanical Engineering, University of Ottawa, Ottawa, ON.
- MAXWELL, B 2016 Turbulent combustion modelling of fast-flames and detonations using compressible lem-les. PhD thesis, University of Ottawa, Ottawa, ON.

- MAZAHERI, K, MAHMOUDI, Y & RADULESCU, M I 2012 Diffusion and hydrodynamic instabilities in gaseous detonations. *Combust. Flame*. **159**, 2138–2154.
- MAZAHERI, K, MAHMOUDI, Y, SABZPOOSHANI, M & RADULESCU, M I 2015 Experimental and numerical investigation of propagation mechanism of gaseous detonations in channels with porous walls. *Combust. Flame* **162**, 2638–2659.
- MCBRIDE, B J & GORDON, S 1996 Computer program for calculation of complex chemical equilibrium compositions. *Technical Report E-8017-1*, National Aeronautics and Space Administration report **Washington D.C.**
- MITROFANOV, V V & SOLOUKHIN, R I 1965 The diffraction of multi-front detonation waves. *Sov. Phys. Dokl.* **9**, 1055–1058.
- MOEN, I O, DONATO, M, KNYSTAUTAS, R & LEE, J H S 1981 The influence of confinement on the propagation of detonations near the detonability limits. *Proc. Combust. Inst.* **18**, 1615–1622.
- MURRAY, S B & LEE, J H S 1984 The influence of yielding confinement on large-scale ethylene-air detonations. *Prog. Astro. Aero* **94**, 80–103.
- MURRAY, S B & LEE, J H S 1986 The influence of physical boundaries on gaseous detonation waves. *Prog. Astro. Aero* **106**, 329–355.
- ORAN, E S, BORIS, J P, YOUNG, T R, FLANIGAN, M, BURKS, M & PICONE, J M 1981 Numerical simulations of detonations in hydrogen-air and methane-air mixtures. *Proc. Combust. Inst.* **18**, 1641–1649.
- ORAN, E S, JONES, A & SICHEL, M 1992 Numerical simulations of detonation transmission. *Proc. R. Soc. Lond. A* **436**, 267–297.
- RADULESCU, M I 2003 The propagation and failure mechanisms of gaseous detonations: experiments in porous-walled tubes. PhD thesis, Department of Mechanical Engineering, McGill University, Montreal, QC.
- RADULESCU, M I & LEE, J H S 2002 The failure mechanism of gaseous detonations: Experiments in porous wall tubes. *Combust. Flame* **131**, 29–46.
- RADULESCU, M. I., SHARPE, G. J. & LAW, C. K. 2007a Effect of cellular instabilities on the blast initiation of weakly unstable detonations. In *Proceedings of the 21st International Colloquium on the Dynamics of Explosions and Reactive Systems*. Poitiers, France.
- RADULESCU, M I, SHARPE, G J, LAW, C K & LEE, J H S 2007b The hydrodynamic structure of unstable cellular detonations. *J. Fluid Mech.* **580**, 31–81.
- ([HTTP://COMBUSTION.UCS.D.EDU](http://COMBUSTION.UCS.D.EDU)) UNIVERSITY OF CALIFORNIA AT SAN DIEGO 2014 Chemical-kinetic mechanisms for combustion applications. *Mechanical and Aerospace Engineering (Combustion Research)*.
- SCHULTZ, E 2000 Detonation diffraction through an abrupt area expansion. PhD thesis, California Institute of Technology, Pasadena, US.
- SHARPE, G J 2001 Transverse waves in numerical simulations of cellular detonations. *J. Fluid Mech.* **447**, 31–51.
- SHEPHERD, J E 1986 *Dynamics of detonations and explosions: Detonations, Vol(106), Chapter: Chemical kinetics of hydrogen-air-diluent mixtures*. University of Colorado at Boulder: Progress in astronautics and aeronautics.
- SHEPHERD, J E 2009 Detonation in gases. *Proc. Combust. Inst.* **32**, 83–98.
- SHORT, M. & BDZIL, J. B. 2003 Propagation laws for steady curved detonations with chain-branching kinetics. *Journal of Fluid Mechanics* **479**, 39–64.
- SHORT, M & SHARPE, G J 2003 Pulsating instability of detonations with a two-step chain-branching reaction model: Theory and modeling. *Combust. Theor. Model.* **7**, 401–416.
- SOW, A, CHINNAYYA, A & HADJADJ, A 2014 Mean structure of one-dimensional unstable detonations with friction. *Journal of Fluid Mechanics* **743**, 503–533.
- STREHLOW, R A & ENGEL, C D 1969 Transverse waves in detonation ii: structure and spacing in H₂-O₂, C₂H₂-O₂, C₂H₄-O₂ and CH₄-O₂ systems. *AIAA Journal* **7**, 492–496.
- SUBBOTIN, V A 1976 Two kinds of transverse wave structures in multifront detonation. *Combust. Explo. Shock Waves*. **11**, 83–88.
- TAKI, S & FUJIWARA, T 1981 Numerical simulation of triple shock behavior of gaseous detonation. *Proc. Combust. Inst.* **18**, 1671–1681.
- VANDERMEIREN, M & TIGGELEN, P J VAN 1984 Cellular structure in detonation of acetylene-oxygen mixtures. *Progress in Astronautics and Aeronautics* **94**, 104–117.

- VASIL'EV, A. A. 1994 Near-limiting detonation in channels with porous walls. *Comust. Explo. Shock Waves* **30**, 101–106.
- VASIL'EV, A. A., GAVRILENKO, T. P. & TOPOCHIAN, M. E. 1972 On the chapman-jouguet surface in multi-headed gaseous detonations. *Astron. Acta.* **17**, 499–502.
- WHITHAM, G. B. 1974 *Linear and nonlinear waves*. New York: Wiley.
- WILLIAMS, F. A. 1985 *Combustion Theory*, 2nd edn. Benjamin/Cummings Publishing Company Inc.
- WOOD, W. W. & KIRKWOOD, J. G. 1954 Diameter effect in condensed explosives - the relation between velocity and radius of curvature of the detonation wave. *Journal of Chemical Physics* **22** (11), 1920–1924.
- WOOD, W. W. & KIRKWOOD, J. G. 1957 Hydrodynamics of a reacting and relaxing fluid. *J. Appl. Phys.* **28**, 395–398.
- YAO, J. & STEWART, D. S. 1995 On the normal detonation shock velocity-curvature relationship for materials with large activation energy. *Combustion and Flame* **100**, 519–528.